The Republic of Iraq
Ministry of Higher Education and
Scientific Research
University of Babylon
College of Sciences for women
Department of Laser Physics

Theoretical Investigation of Optoelectronics Properties of Oligo(phenylene-ethynylene) Molecules for dye Organic Laser

A Thesis

Submitted to the Council of the College of Sciences for Women,

University of Babylon

In Partial Fulfillment of the Requirements for the Degree of

Master in Laser Physics and its Applications

BY

Noor Median Adheem

Supervised by

Assistant. Prof. Dr. Oday A. Al-Owaedi

2022 A.D **1443 A.H**

بِسْمِ اللَّـهِ الرَّحْمَـٰنِ الرَّحِيمِ

لَا الشَّمْسُ يَنْبَغِي لَهَا أَنْ تُدْرِكَ الْقَمَرَ وَلَا اللَّيْلُ سَابِقُ

النَّهَارِ وَكُلٌّ فِي فَلَكٍ يَسْبَحُونَ(40)

صَدق الله العلي العظيم

سورة يس

Declaration

I hereby declare that the thesis is my own work and effort and has not been submitted in substantially the same form for the award of a higher degree elsewhere. Other sources of information have been used, they have been acknowledged. This thesis documents work carried out between October 2021 and September 2022 at the University of Babylon, Iraq, under the supervision of Assistant Prof. Dr. Oday A. Al-Owaedi.

Noor

Dedications

To

This thesis is dedicated to my mother. Without her endless love and

encouragement I would never have been able to complete my

graduate studies. I love you and I appreciate everything

that you have done for me.

Also to my father I am truly grateful for having inmy life.

This thesis is also dedicated to my sisters and my brother, (Abeer,Roaa,farah and mohammed)

To gave me lots of

support.

To my friends and colleagues who helped me

Noor

Acknowledgment

This thesis would never completed without the excellent supervision and guidance I received from **Assistant Prof. Dr. Oday A. Al-Owaedi.** There are no words in English books can express my gratitude to you. Really you were excellent supervisor.

I am deeply indebted to the Head of the Laser Physics Department, the staff and the dean of the College of Science for Women for the support that provided.

Also I would like to pay my regards to all relatives and friends for the help they showed at the Department of Laser Physics.

I would like to express my very deep respect and sincere appreciation to my family, whose patience and moral encouragement gave me so much hope and support.

Above all, my great thanks to **ALLAH** for his mercy and blessing.

Noor

Abstract

Understanding charge transport of single molecules sandwiched between electrodes is of fundamental importance for molecular electronics. The structural properties of oligo (phenylene-ethynylene)(OPE) with five different anchor groups (thiol (SH), pyridine (PY), methyl sulfide (SMe), tetramethylsilane (TMS) and dibenzothiophene (DBT)).The optimized molecular junction geometries conform well to a description of the SH, SMe and BDT contacted compounds forming an angle of 52° contact between anchor groups and the undercoordinated gold atoms of the gold electrodes. In addition, it shows that PY and TMS contact groups create an angle of 160°.Undoubtedly, these structural aspects will affect the junction formation probability and all other properties (electronic, electric, thermoelectric and spectral) of these molecules. On the other hand,The transmission coefficient value of all molecules was high. This can understand in terms of the quantum interference is a constructive interference and there is no a destructive interference signature, and that (OPE-1) introduces a high value of transmission coefficient (5.8×10^{-4}), while the lowest value of the transmission (3.12×10^{-6}) is presented by molecule (OPE-4). The molecule OPE-4 with TMS anchor gropus produces the highest f_{em} (2.4), while the molecule (OPE-2) with PY contact groups shows the lowest f_{em} (1.8). In addition, it could be observed that the

maximum wavelength (λ_{max}) for all molecules lies in the UV region, and there is also a fluctuation from 349.7 nm for OPE-2 to 383.6 nm for OPE-5.Also, the thiol-terminated molecular junctions (OPE-1) have a positive Seebeck coefficient that show the HOMO. In contrast, SMe, DBT, PY and TMS-terminated molecular junctions have a negative Seebeck coefficient and conduct through the LUMO. The molecule with SH anchor groups (OPE-1) gives the hieghest electronic properties and lowest thermoelectric properties. In contrast, the molecule with TMS anchor groups (OPE-4) produces the hieghest thermoelectric properties and the lowest electronic characteristics.

Table of Contents

Chapter 1 : Introduction

Chapter 2 : Density Functional Theory

Table of Contents

List of Abbreviations

Abbreviation	Physical meaning
OLEDs	Organic Light Emitting Diodes
SPM	Scanning Probe Microscopy
STM-BJ	Scanning Tunnelling Microscopy Break Junctions
MCBJ	Mechanically Controllable Break Junctions
OSSL	Organic Solid-State Lasers
ASE	Amplified Spontaneous Emission
DFT	Density Functional Theory
TD-DFT	Time-Dependent Density Functional Theory
UV	Ultra-violet
NIR	Near-infrared
NUV	Near- Ultra-violet
HOMO	High occupied molecular orbitals
LUMO	Lowest unoccupied molecular orbitals
SIESTA	Spanish Initiative for Electronic Simulations with Thousands of Atoms
KS	Kohn and Sham
LDA	Local density approximation
GGA	Generalized gradient approximation
PBE	Perdew, Burke and Ernzherhof
LCAOs	Linear Combination of Atomic Orbital
R-G	Runge-Gross theorem
GF	Green‘s function
OPE	Oligo(phenyleneethynylene)
SH	Thiol
PY	Pyridine
SMe	Methyl sulfide
TMS	tetramethylsilane
DBT	dibenzothiophene
FMOs	Front molecular orbitals
B.E.	Binding energy
LCAOMO	linear combination of atomic orbitals Molecular orbitals

BSSEC	Basis set superposition error correction
FET	field-effect transistor

List of Symbols

Symbol	Physical Meaning
m_n	Mass of the nucleus
Z_m	Atomic number
R_n	Position
T_e	Kinetic energy of the electron
T_n	Kinetic energy of the nuclei
U_{ee}	Interaction energy between all electrons
f_{em}	Emission oscillator strength
Ψ	Wave function
n(r)	Ground-state density
$\hat{H}$	Hamiltonian operator
M	Nuclei number
$\boldsymbol{N}$	Electrons number
r_i	Position of the *i-th* electron
R_I	Position of the I-th nucleus
E_i	Numerical value of the energy of the i^{th} state
U_{nn}	Interaction energy terms between the nuclei
U_{en}	energy between electrons and nuclei
m_e	Mass of the electron

e	Electron charge
Z_n	Nuclear charge
r_i	Position of the electrons
R_n	Position of the nuclei
∇_i^2	Laplacian operator
$V_{ext}(\vec{r})$	External potential
H_{eff}	Effective Hamiltonian
V_{eff}	Effective external potential
$F_{K-S}[n(\vec{r})]$	Energy functional of the Kohn-Sham
E_{xc}	Exchange-correlation energy
E_X	Exchange energy of an electron
E_C	Correlation energy of an electron
$s = \frac{\lvert V\rho \rvert}{2k_{F\rho}}$	Dimensionless density gradient
k_{T-F}	Thomas-Fermi screening wavenumber
r_s	Local Seitz radius
r_c	Core radius
r	Outside of the core radius
V_{nl}^{ps}	Pseudo-potential
R_{nl}^{ps}	Radial pseudo-wavefunction
$\Psi_{nlm}^{I}(r)$	Single basis function

R_{nl}^{I}	Radial wavefunction
Y_{lm}^{I}	Spherical harmonic
φ_i	Molecular orbitals (basis functions)
μ_L	Chemical potential in the left
μ_R	Chemical potential in the *right*
T(E)	Probability the transition
R	Probability the reflection
δI^{in}	Incident electric current
ε_o	on-site energies
$-\gamma$	Hopping parameters
k	Wavenumber
ε_1	Single site energy
ε_2	Two site energy
$\Gamma_{L,R}(E)$	Level broadening due to the coupling between right (R) and left (L) electrodes
$\mathcal{T}_L$	Temperature left
$\mathcal{T}_R$	Temperature right
Γ	Number of transfer electrons
e_J	Number of electron on nitrogen atoms when molecule in a junction
e_N	Number of electron on nitrogen atoms when molecule in gas-phase

δV	Voltage associated with the chemical potential mismatch
G	conductance
S	Matrix, it connects states coming from the left lead to the right lead and vice versa:
$\Delta \mathcal{T}$	Temperature
ΔV	Potential drop
I	Charge current
$\mathcal{Q}$	Heat current
ZT_e	Electronic figure of merit
E_F	Fermi energy
$f(E)$	Fermi-Dirac function
f_L	Fermi distribution from the left
f_R	Fermi distribution from the right
$S(T)$	Thermo electric power
G/G_0	Electrical conductance
G_o	Quantum of conductance
h	Planck's constant
K_B	Boltzmann constant
ε	Absorption intensity
λ_{Max}	Maximum wavelength
A	Absorption intensity

E	Emission intensity

List of Figures

List of Tables

Chapter One

Introduction

1.1. Introduction

Molecular electronics has attracted great attention from a wide variety of researchers, due to promising applications in nanoscale electronic devices such as transistors [1], switches [2], rectifiers, interconnects [3], organic photovoltaic and chemical sensors. Using molecules as electronic elements has many advantages due to their small sizes, their ability to be self-assemble onto surfaces and the low cost of producing large numbers of identical molecules. However, realizing and controlling the connection between the molecule and electrodes has remained challenging due to small molecular size [4].

The use of individual molecule as functional electronic devices was first proposed in the 1970s [5]. In order to design and realize molecular devices it is essential to have a good understanding of the properties of an individual molecule. Within the framework of molecular electronics, the most important property of a molecule is its conductance and the major question in this field is how electrons move through molecules. To address this question, extensive experimental and theoretical studies have been carried out. Various measurement techniques have been developed [6].

The field is currently attracting attention from a broad cross-section of the scientific community in response to both fascinations with the fundamental scientific challenges associated with the measurement of the electrical

properties of molecules, and manipulation of electronic phenomena via molecular processes, and growing concerns over the technological challenges and ultimate limits facing solid state semiconductor technology. The use of organic materials for electronic applications in which the bulk electronic or optoelectronic response arises from ensembles of several millions of molecules, and for which properties are measured or observed on the macroscopic level, is at a mature stage of development and application. The most obvious examples of molecular materials readily available in the electronics mass market are the use of liquid crystals and organic light emitting diodes (OLEDs) in flat video displays [7]. This sector of the electronics industry continues its steady development driven by the promises of transparent, flexible, non-toxic, printable electronics, with improved consumer. In molecular electronic junctions, the electrical signal comes in and out of the molecules via contact-coupled electrodes. The electrodes can be classified as metal or nonmetal electrodes. The development of molecular electronics initially started from the use of metal electrodes. Hence, the development of molecular devices based on metal electrodes will summarized [8].

1.2. Single Molecule Junctions

The initial idea of using individual molecules as active electronic elements provided the impetus to develop a variety of experimental platforms to probe their electronic transport properties. Among these platforms, single-molecule junctions based on metal−molecule−metal architecture have received considerable attention and contributed significantly to the fundamental understanding of the physical phenomena required to develop molecular-scale electronic devices. The scanning probe microscopy, SPM, technique is regarded as a milestone in the history of molecular electronics because it has made a great contribution to the development of molecular electronics and continues to promote the advancement of molecular electronics in the future. In addition to SPM technique, Scanning Tunnelling Microscopy Break Junctions (STM-BJ) [9-11] and Mechanically Controllable Break Junctions MCBJ [12, 13] have been used widely.

Generally, materials used as electrodes in molecular junctions should have superior properties in four aspects. The first premise is good electrical conductivity, which can maintain its high value with dimension scale-down. The second is the stability of the material composition and configuration, which is of great importance for resisting external perturbation/oxidation and ensuring the success of forming molecular junctions. The third is the

abundant availability using either bottom-up or top-down approaches [14]. The fourth is the ease of material processing, which should be compatible with industrial micro/nanofabrication techniques. On the basis of these considerations, the past two decades have witnessed a large variety of materials being used in molecular electronics, ranging from conventional noble metals to novel carbon allotropies, which continuously and creatively update the paradigms for device architecture and operation. In addition to the materials mentioned above, there were also other attempts to expand the research regimes of molecular electronics, including silicon and polymer-based nanoelectrode systems as silicon-based electrodes [13], and Complementary‑Metal‑Oxide‑Semiconductor(CMOS)compatibleelectrode, such as Pt and Pd [14].

1.3. Integrating Molecular Functionalities into Devices

Undoubtedly, the substantial experimental and theoretical progress detailed above lays the foundation for both the measurement capabilities and a fundamental understanding of the various physical phenomena of molecular junctions. Despite these considerable achievements, there are still no commercially available molecular electronic devices [14]. To satisfy the requirements for actual applications, the development of practical molecular devices with specific functions is a prerequisite. In fact, recent experimental

rectification as well as how quantum interference effects play a critical role in the electronic properties of molecular junctions [15]. The focus of these experiments illustrates the engineering of functionalities that are beyond conventional electronic transport properties using a rational chemical design in single-molecule junctions. The developing trends of integrating molecular functionalities into electrical circuits based on single molecules is including a wiring toward nanocircuits; rectification toward diodes; modulation toward transistors; switching toward memory devices; and transduction toward sensors [16]. For different functions resulted from individual molecules, both molecular cores and molecular tails are equally important due to the fact that the proposed functions could be affected not only by molecular electrical characteristics but also by the electrode−molecule bonding. In summary, with the rapid development of molecular-scale electronics, using molecular devices as the future of next-generation electrical circuit units with lower power consumption, higher speed, and higher level of integration has received significant attention [17].

1.4. Organic Molecules

Organic molecules are chemical compounds with complicated structures. Composed of many atoms, apart from electronic properties they also exhibit special physicochemical features [18]. When organic molecules created molecular solid-state devices with crystal or amorphous structures, the properties of these devices follow from organic molecule interactions. Therefore, in molecular solid-state structures, the energy levels of individual molecules form continuous bands of energy. Due to the weak interactions between the molecules, molecular solid-state structures exhibit the properties of the individual molecules to a greater degree than the properties characteristic for solid-state materials [19]. A special feature of the molecular solid state is the fact that singlet and triplet states are excited due to light interaction being able to move across the material. These mobile quasi-particles are called excitons. Furthermore, excitons can be generated not only by light but also from the recombination process of charge carriers with opposite signs, electrons and holes injected into the system [20]. This has important implications and enables the application of organic materials to light-emitting devices able to produce any colour. Owing to the excitation of the organic material by electromagnetic waves with energy, carriers are

generated. Taking into account these features of organic materials, it could be conclude that they have significant potential in many fields of science and technology. Therefore an understanding of their properties is salient, and our current knowledge remains insufficient [21].

1.5. Electrical Pumping of Organic Laser Active Medium

Organic solid-state lasers (OSSL) have received a lot of attention in recent years due to their ease of manufacture and ability to cover a broad range of lasing wavelengths from near infrared to ultraviolet. Optically pumped OSSL have progressed to the point that they can reach impressively low thresholds for laser and/or amplified spontaneous emission (ASE), as well as operation that is almost constant. However, the ultimate aim in the field of OSSL is to achieve electrically pumped lasing, which will allow for the development of low-cost, portable, and flexible solid OSSL devices [6,7].

Because of the following considerations, electrically pumped OSSL lasing is far more difficult than optically pumped OSSL lasing. First, a ccording to spin statistics, three-quarters of excitons generated during current injection are triplets, which have a lengthy decay period [22]. Second, polarons, excitons, and other species that are not engaged in optical pumping will cause repeated annihilation and absorption losses when electrical pumping is used. The recent advances have reported promising signs of current injection OSSL, which has opened up the possibility of

developing small and low-cost electrically powered organic laser systems [23]. Regardless of these organic laser gain medium, electrical pumping was used to investigate light amplification. As a result, it's crucial to conduct theoretical analysis and forecast potentially good electrical pumping options, which must have a large stimulated emission cross section, low annihilation or absorption losses, and a short lifetime, ideally with high mobility [7]. In this context, the purpose of this communication is to offer an universal computational approach for systematically screening out electrically pumped lasing molecules over a broad spectrum of organic solid-state luminous materials using efficient electronic structure computations based on density functional theory (DFT) and time-dependent DFT (TD-DFT) [23,24].

Organic dyes absorb light in the ultraviolet (UV) to near-infrared (NIR) spectral range. Multiple conjugated double bonds are present in all of these compounds, limiting their spectral characteristics and chemical reactivities. The large range of chemical configurations that may operate as laser dyes is one of the major reasons for dye lasers' surge in popularity. Laser dyes emit light over the whole visible spectrum, as well as the NUV and NIR spectral regions. more than 500 distinct dyes with varying absorption and emission bands may be discovered. Laser dyes are typically classified according to their chemical structures [24].

1.6. Literature Review

Changsheng Wang et al, in 2009 [25], have used STM-molecular break junction methods in Au|molecule|Au configurations, the electrical conductivity of the oligoyne molecular wires Py-(CtC)n-Py (n) 1, 2 and 4; Py) 4-pyridyl) was investigated at the single molecule level. Multiple series of peaks can be seen in the conductance histograms, which can be attributed to different contact geometries between the pyridyl head groups and the gold electrodes. Higher conduction groups are linked to pyridyl group adsorption at more strongly coordinated places such as step edges or adjacent gold adatoms, according to both experimental and theoretical data. *Pavel Moreno-García et al, in 2013* [26], have reported that the electrical conductivity of a series of oligoyne molecular wires in single-molecule junctions with gold contacts was investigated using a combination of experimental and theoretical methods. The synthesis and characteristics of diaryloligoynes with n = 1, 2, and 4 triple bonds, as well as the anchor dihydrobenzo[b]thiophene, are the subjects of their experiments (BT). The aurophilic anchor groups cyano (CN), amino (NH2), thiol (SH), and 4-pyridyl were also investigated for comparison (PY). To explore single-molecule conductance characteristics, researchers used scanning tunneling

microscopy break junction (STM-BJ) and mechanically controlled break junction (MCBJ) methods.

Oday A. Al-Owaedi et al in 2016 [27], have introduced a theoretical and experimental studies of trans-Ru complexes. They interpreted the electronic properties of such molecules in terms of the transport mechanisms (LUMO-dominated conductance). These results have significant implications for the future design of organometallic complexes for studies in molecular junctions. In comparison to the typical anchoring groups that have been studied thus far, the BT moiety outperforms them. BT-terminated oligoynes have a 100% chance of forming a junction and have the greatest conductance values of all the oligoynes examined, as well as greater conductance values than other conjugated molecular wires of comparable length. For oligoynes with n = 14 triple bonds, DFT calculations are provided. Each family of molecules has its own set of conductance traces and conductance distributions.

Oday A. Al-Owaedi et al in 2017 [28], have highlighted research on the critical role of metal complexes in preventing orthogonal contacts, which helped to explain why some organometallic compounds had very high conductance values.

Mohsin K. Al-Khaykanee et al in 2018 [29], have work that comprised a study of the charge transport of 4,4-bipyridine molecules with a variety of sterically-induced twist angles between the two pyridyl rings, which was

done using density functional theory DFT and Green's function formalism. Different molecular orientations within the junctions were shown to be the cause of high and low conductance peaks, according to one experiment. The conductances of both geometries were proportional to twisted angle demonstrating that the electrical current travels through the C-C bond joining the pi systems of the two rings.

Guang-Ping Zhang et al in 2019 [30], have studied theoretically by using the perturbation theory the impact of bridging for DHP/CPD photoswitchable molecule sandwiched between two Au(111) electrodes. Due to their differing alignments of HOMO with E_F, their numerical findings show a clear switching effect for DHP/CPD, with the fully conjugated DHP being more conductive (ON state), than the less conjugated CPD (OFF state). The ON/OFF switching ratio is also discovered to be considerably influenced by the bridging method. Further investigation demonstrates that the contributions of local bonds to the transmission channel are substantially tied to the core molecule's conjugation properties and may be significantly altered by the bridging method.

Masoud Baghernejad et al in 2020 [31], have mentioned that the influence of heteroatoms on electron transport via asymmetric and symmetric alkyne-terminated benzodichalcogenophene compounds has been investigated using a combination of experimental and theoretical methods. Experiments, DFT-based theory, and a simple tight binding model were all in excellent

agreement. The decreased conductance of the asymmetric molecule is caused by the asymmetry created by differing bond lengths in the two 5-membered rings of the molecule, as demonstrated by the tight-binding modeling of heteroatom replacement in these non-bipartite cores. In addition, they discover that the differing overlap integrals of the CO and C-S bonds must be taken into consideration in the tight binding model.

Yi Jiang et al in 2020 [32], have studied a variety of gain materials including organic dyes, fluorescent semiconductor emitters, triplet gain media, and biological materials, covering a wide spectrum from UV to NIR. Some gain media are already commercial available, including some laser dyes, i.e. TDAF-1 (79), PFO (203), F8BT (225) and bis-styrylbenzene), introducing branched flexible chains, constructing triplet gain media and triplet harvesters, may be beneficial to the development of robust organic gain media for OSLDs. They hope that in the future, intense efforts will be paid to explore various successful ways to realize electrically pumped organic lasers and promote their practical application, inspired

by the recent advancements.

Baraa A. Al-Mammory et al in 2021 [33], have studied Oligoynes, which are prototype molecular wires due to their conjugated system and the coherent tunneling transport, which aids this type of wires to transfer charges over long distances. The electric and thermoelectric characteristics for a series of Oligoyne molecular wires ((n) 3, 5, 7 and 9) are studied to explore the

fundamental transport mechanisms for electrons crossing single molecules. They have probed both the electrical conductance and Seebeck coefficient for Au|molecule|Au configurations using the density functional theory (DFT). The results not only confirmed the expected exponential decrease of conductance with the number n of triple bonds, according to the formula $G_n = Ae^{-\beta n}$, but also demonstrated that the linear increase in the Seebeck coefficient S_n with increasing number of triple bonds.

Rasool M. Al-Utayjawee et al in 2021 [34], have studied the applications of single-molecule porphyrin based strucuters by using molecules as elementary blocks of electronic components involving metallic atoms. Theoretically, one type of molecular-scale porphyrin device is used in this article, consisting of organometallic single molecules with different metals (Zn, Mg, Cu and Fe), sandwiched between gold electrodes bound by thiol anchor groups. The transmission and Seebeck coefficients for Au|molecule|Au configurations were computed by using density functional theory (DFT). The findings show that there is a robust Fano resonance in the transport behaviour around the Fermi energy, only for the porphyrin-based device with Fe metal. This result is attributed to the destructive quantum interference between continuous and discrete states. This work not only indicates that there is a relationship between the electrical conductance and thermo power but also it introduces a promising strategy to affect and control these characteristics via creation of Fano phenomenon.

M. Naher, et al., in 2021 [35], have studied a series of 12 conjugated molecular wires, 6 of them contain either a ruthenium or platinum center centrally placed within the backbone. The measurements and calculations have demonstrated a small positive Seebeck coefficient, and the transmission coefficient through these molecules takes place by tunneling through the tail of the HOMO resonance near the middle of the HOMO–LUMO gap in each case.

1.7. Thesis Outline

The outline of this thesis can be summarized as follows; this chapter is followed by chapter 2 which presents a brief overview of density functional theory (DFT), which is one of the main theoretical techniques that has used in this thesis to study and understood the electronic properties of single-molecule junctions. Furthermore, it describes the single particle transport theory, which involves a Green's function scattering formalism and all related topics such as the Landauer formula. Chapter 3 represents the results and discussions of the electronic, thermoelectric, optical and spectral properties of variety of molecles. Chapter 4 illustrates the conclusions of this study.

1.8. The Aims of the Study

The goals of this work can be summarized as following:

1. Study of electronic, electric, thermoelectric and some of optical properties of a series of all molecules in this work.
2. Obtaining the fundamental understanding of the effect of many factors and their impact on the characteristics of these simple prototypical systems such as the molecular length and the kind of anchor groups.
3. Conducting analysis of work results and providing forecasts for the use of these nanostructures in the field of optoelectronics applications

Chapter Two

Theories and Models

2.1. Introduction

In an attempt to explore and understood the electronic properties of molecules, many theories have emerged; one of the most important of these theories and most common is the density functional theory (DFT). Nowadays, DFT can be presented as a powerful tool for computations of the quantum state of atoms, molecules and solids, and of ab-initio molecular dynamics. In 1927, immediately after the foundation of quantum mechanics, an initial and approximate version of density functional theory was conceived by Thomas and Fermi [36]. Later, using the basics of quantum mechanics, Hohenberg, Kohn, and Sham, developed density functional theory of the quantum ground state to be superior to both Thomas-Fermi and Hartree-Fock theories, which opened a wide door to the applications for realistic physical systems [37, 38]. From that time on, density functional theory (DFT) has grown vastly, and it has become one of the main tools in theoretical physics and molecular chemistry.

This chapter presents a brief summary of DFT and SIESTA (Spanish Initiative for Electronic Simulations with Thousands of Atoms) code [39], which has been used to study the electronic, electric, spectral and thermoelectric properties of the molecules that are the subject of research in this thesis [40].

2.2. The Many-Body Problem

This is an approach which aims to solve any system consisting of a large number of interacting particles. In a microscopic system consisting of charged nuclei surrounded by electron clouds these interactions such as electron-nuclei, electron-electron, nuclei-nuclei and electron correlations are described via Schrödinger equation [40].

The full Hamiltonian operator of a general system describing these interactions is

$$\hat{\mathrm{H}} = \overbrace{-\frac{\hbar^2}{2m_e}\sum_{i=1}^{N}\nabla_i^2}^{T_e} \overbrace{-\frac{\hbar^2}{2m_n}\sum_{n=1}^{M}\nabla_n^2}^{T_n} \overbrace{-\frac{1}{4\pi\varepsilon_o}\sum_{i=1}^{N}\sum_{n=1}^{M}\frac{1}{\left|\vec{r}_i-\vec{R}_n\right|}Z_n e^2}^{U_{en}}$$
$$+\frac{1}{4\pi\varepsilon_o}\frac{1}{2}\overbrace{\sum_{i=1}^{N}\sum_{i\neq j}^{N}\frac{e^2}{\left|\vec{r}_i-\vec{\vec{r}}_j\right|}}^{U_{ee}}+\overbrace{\frac{1}{4\pi\varepsilon_o}\frac{1}{2}\sum_{n=1}^{M}\sum_{n\neq n'}^{M}\frac{1}{\left|\vec{R}_n-\vec{R}_{n'}\right|}Z_n Z_{n'}e^2}^{U_{nn}} \quad (2.1)$$

Here i and j denote the N-electrons while n and n' run over the M-nuclei in the system, m_e and m_n are the mass of electron and nucleus respectively, e and Z_n are the electron and nuclear charge respectively. The position of the electrons and nuclei are denoted as $\vec{r}_i$ and $\vec{R}_n$ respectively,

Approximately, the mass of nucleons is a few orders of magnitude higher than that of electron, and in terms of their velocities, the nuclei could be considered as a classical particle which creates an external potential, and the electrons as quantum particles are subjected to this potential.This concept is known as the Born-Oppenheimer approximation [40], together with an assumption that the nucleon wavefunction is independent of the electron position, equation (2.1) can then be written as follows:

$$H = T_e + U_{e-e} + V_{e-nuc} \tag{2.2}$$

The first part of equation (2.2) presents the kinetic energy of all electrons, which is described by;

$$T_e = \sum_n \frac{\hbar 2}{2me} \nabla_i^2 \tag{2.3}$$

The electron-electron interaction is represented in the second part of equation (2.2), which is given by;

$$U_{e-e} = \sum_{i,j,i\neq j} \frac{e^2}{4\pi\varepsilon_0} \frac{1}{|\vec{r}_i - \vec{r}_j|} \tag{2.4}$$

$Ue{-}e$ describes the sum of all potentials acting on a given electron at position $r_i$by all other electrons at position r_j .

The third part of equation (2.2) describes the interactions between electrons and nuclei, which is expressed by;

$$V_{e-nuc} = \sum_i \sum_n \ v_{nue}(r_i \ - R_n \ ) \tag{2.5}$$

v_{e-nue} is the interaction between electrons and nuclei; it depends on the positions of electrons r_i and nuclei R_n .

The employment of a Born-Oppenheimer approximation [40], allows the electron and nucleon degrees of freedom to be decoupled.

2.3. The Hohenberg-Kohen Theorems

Essentially, density functional theory (DFT) evolved significantly depending on two ingeniously simple theorems put forward and proved by Hohenberg and Kohn in 1964 [37]. These theorems are two powerful statements:

Theorem I: For any system of interacting particles in an external potential V_{ext}, the density is uniquely determined. In other words, the external potential is a unique functional of the density. To prove this theorem, assume that there are two external potentials $V_{ext}{}^{(1)}$ and $V_{ext}{}^{(2)}$ differing by more than a constant, and giving rise to the same ground state density, $\rho_0(r)$. It is clear that these potentials belong to different Hamiltonians, which are denoted H^1 and H^2 they give rise to distinct ground-state wavefunctions $\psi^{(1)}$ and $\psi^{(2)}$. Since $\psi^{(2)}$ is not a ground state of $H^{(1)}$, so:

$$E^{(1)} = \langle\psi^{(1)}|H^{(1)}|\psi^{(1)}\rangle < \langle\psi^{(2)}|H^{(1)}|\psi^{(2)}\rangle \quad (2.6)$$

and, similarly:

$$E^{(2)} = \langle\psi^{(2)}|H^{(2)}|\psi^{(2)}\rangle < \langle\psi^{(1)}|H^{(2)}|\psi^{(1)}\rangle \quad (2.7)$$

Assuming that the ground states are non-degenerate [41,42], one could rewrite equation (2.6) as follows:

$$\langle \Psi^{(2)} \left| H^{(1)} \right| \Psi^{(2)} \rangle = \langle \Psi^{(2)} \left| H^{(2)} \right| \Psi^{(2)} \rangle + \langle \Psi^{(2)} \left| H^{(1)} - H^{(2)} \right| \Psi^{(2)} \rangle$$

$$= E^{(2)} + \int \left(V_{ext}^{(1)}(r) - V_{ext}^{(2)}(r) \right) \rho_0(r)\, dr \qquad (2.8)$$

and assuming that $|\Psi^{(1)}\rangle$ has the same density $\rho_0(r)$ as $|\Psi^{(2)}\rangle$:

$$\langle \psi^{(1)} \left| H^{(2)} \right| \psi^{(1)} \rangle = E^{(1)} + \int \left(V_{ext}^{(2)}(r) - V_{ext}^{(1)}(r) \right) \rho_0(r)\, dr \qquad (2.9)$$

Combining of equations (2.8) and (2.9) leads to,

$$E^{(1)} + E^{(2)} < E^{(1)} + E^{(2)} \qquad (2.10)$$

This equation proves the two different external potentials cannot produce the same ground-state density.

Theorem II: A universal functional $F[\rho]$ for the energy $E[\rho]$ could be defined in terms of the density. The exact ground state is the global minimum value of this functional. In other words, the ground state energy of the system is given by the functional $F[\rho]$. If the input density and ground-state density are the same, the functional $F[\rho]$ would deliver the lowest energy. Hence, the functional could be minimised by varying the density to obtain the ground-state energy for the external potential [41].

The second theorem could be proven by considering the expression for the total energy, E, of the system with density ρ.

$$E[\rho] = T[\rho] + E_{\text{int}}[\rho] + \int V_{\text{ext}}(r)\rho(r)dr \qquad (2.11)$$

The kinetic energy term, T, and internal interaction energy of the electrons, E_{int}, depend only on the charge density, and so are universal[42].

The first theorem reported that the ground-state density (ρ_0) for a system with external potential (V_{ext}) and wavefunction (Ψ_0), determines the Hamiltonian of that system, so for any density, ρ, and wavefunction, Ψ, other than the ground state, it could be found:

$$E_0 = \langle \Psi_0 | H | \Psi_0 \rangle < \langle \Psi | H | \Psi \rangle < E \qquad (2.12)$$

Hence, the ground-state density, $\rho 0$, minimizes the functional (equation 2.11). If the functional $T[\rho]+E_{int}[\rho]$ is known, then by minimizing equation 2.11, the ground-state of the system could be obtained, and then all ground-state characteristics could be calculated, which are the subject of the interest[42].

2.4. The Kohn-Sham Method

The Kohn-Sham method has been used in solid state physics for about fifty years. By now, largely due to the development of increasingly accurate density functionals, the method has also gained a large popularity among physicist and chemists, especially as it allows in many cases, accurate treatments of molecular systems unattainable by the more traditional quantum mechanical methods [43,44].

It has been reported in the previous section that obtaining the ground-state density leads to calculating the ground-state energy. However, the precise form of the functional shown in equation (2.11) is not known. Generally, the kinetic term and internal energies of the interacting particles cannot be expressed as functionals of the density.

Kohn and Sham in 1965 [38], came up with the idea, that it possible to replace the original Hamiltonian of the system by an effective Hamiltonian of non-interacting particles in an effective external potential, which gives rise to the same ground state density as the original system [45,46].

The form of energy functional of the Kohn-Sham ansatz is:

$$E_{KS}[\rho] = T_{KS}[\rho] + \int V_{ext}(r)\,\rho(r)dr + E_H[\rho] + E_{xc}[\rho] \qquad (2.13)$$

Here, T_{KS} is the kinetic energy of the non-interacting system. The kinetic energy, *T*, in equation (2.11) has been used for the interacting system. This discrimination is due to the exchange correlation, E_{xc}, functional, which is described in equation (2.15). E_H is the Hartree functional, which describes the electron-electron interaction using the Hartree-Fock method [47,51], and it is given by:

$$E_{\mathrm{H}}[\rho] = \frac{1}{2}\iint \frac{\rho(r)\rho(r')}{|r-r'|}\,dr\,dr' \qquad (2.14)$$

This is an approximated version of the internal interaction of the electrons, E_{int}, as defined previously. Again, the difference referred to the exchange correlation, E_{xc}. Therefore, the differences between the exact and

approximate solutions for the kinetic energy, and electron-electron interaction terms were represented via E_{xc}, which is expressed by:

$$E_{xc}[\rho] = (E_{int}[\rho] - E_H[\rho]) + (T[\rho] - T_{KS}[\rho]) \qquad (2.15)$$

Consequently, the Kohn-Sham method could be a powerful approach to obtain an accurate ground-state density if the exchange correlation, E_{xc}, is known precisely [51].

2.5. The Exchange Correlation Functionals

The biggest challenge of Kohn-Sham DFT is the finding of accurate approximations to the exchange correlation energy, Exc. The best understanding of exact functional could be obtained by the best approximation could be designed it [52]. Many efforts have been spent to find the best approximation for the exchange-correlation functional, and numerous forms have been proposed. This section presents a brief summary of two of the most popular approximation forms. The first one is the local density approximation (LDA) [53]. Secondly, the generalized gradient approximation (GGA) [54]. The comparison in terms of the accuracy between LDA and GGA, reported that the GGA is more accurate approximation, because it is designed based on density and the density gradients, while LDA is the simplest, because it is based on the local density.

2.5.1. Local Density Approximation

The simplest approximation is to assume that the density can be treated as a uniform electron gas. Based on this approximation, which was initially proposed by Kohn and Sham [38], the exchange-correlation energy for a density ρ is given by:

$$E_{XC}^{LDA}[\rho] = \int \rho(r)(\epsilon_x^{hom}(\rho(r)) + \epsilon_c^{hom}(\rho(r)))dr \qquad (2.16)$$

Here, the terms ϵ_x^{hom} and ϵ_c^{hom} are the exchange and correlation energy densities for the homogeneous electron gas. The analytical exchange energy, ϵ_x^{hom}, can be found in the literature [55]:

$$\in_x^{hom} = -\frac{3}{4\pi}\sqrt[3]{3\pi^2\rho} \qquad (2.17)$$

Ceperley and Alder [56] calculated numerically the correlation energy $\in_C^{hom}$ using the quantum Monte-Carlo method, then Perdew and Zunger [57] fitted the numerical data to analytical expressions, and found:

$$\in_c^{hom} = \begin{cases} -0.048 + 0.031\,ln(r_s) - 0.0116\,r_s + 0.002\,ln(r_s) & \text{rs} < 1 \\ -\dfrac{0.1423}{(1 + 1.9529\sqrt{r_s} + 0.3334\,r_s} & r_s > 1 \end{cases} \qquad (2.18)$$

Here, $r_s = (\frac{3}{4\pi\rho})^{-1/3}$ is the radius of a sphere in a homogeneous electron gas of density, ρ that contains one electron.

The LDA is often surprisingly accurate and for systems such as graphene and carbon nanotubes or where the electron density slowly varies, generally gives very good results. Despite the remarkable success [58,59], of the LDA, care should be taken in its application. For example, LDA predicts a wrong ground state for the titanium atom and it gave a very poor description for hydrogen bonding [60,61], as well as it gives an incorrect value of the band gap in semiconductors and insulators [62,63].

2.5.2. Generalized Gradient Approximation

The pitfalls of the local density approximation (LDA) and a fact that real systems are inhomogeneous, means that there is a need to find an alternative approximation, which is the generalized gradient approximation (GGA). Basically, there is no analytical form for the exchange energy in GGA, and therefore it has been calculated along with the correlation term, numerically. Nowadays, there are various parameterizations which are used in this approximation; one of the most popular and most reliable is the PBE functional form, which was proposed in 1996 by Perdew, Burke and Ernzherhof [64]:

$$E_{XC}^{GGA} = E_X^{GGA}[\,r] + E_C^{GGA}[\,r] \qquad (2.19)$$

The exchange part is given by:

$$E_X^{GGA} = \int \in_X \big(\rho(\,r)\big) V_X \big(\rho(\,r), \nabla\rho(\,r)\big)\rho(\,r)dr \qquad (2.20)$$

Where,

$$V_X(\rho, \nabla\rho) = 1 + k - \frac{K}{1+\frac{\mu S^2}{K}} \quad (2.21)$$

The values of k and μ parameters are 0.804 and 0.21951, respectively and $s = \frac{|\nabla\rho|}{2k_F\rho}$ is the dimensionless density gradient and k_F is the Fermi wavelength and $V_x(\rho,\nabla\rho)$ represents the enhancement factor[61].

The correlation energy form is given by:

$$E_C^{GGA}[\rho] = \int \rho(r)[\epsilon_c(\rho(r)) + F(\rho(r), \nabla\rho(r))]dr \quad (2.22)$$

$$F(\rho, \nabla\rho) = \frac{\gamma e^2}{a_0} \ln\left[1 + \frac{\beta t2}{\gamma}\left(\frac{(1+At^2}{1+At^2+A^2t^4}\right)\right],$$

$$A = \frac{\beta}{\gamma}\frac{1}{(\exp -\frac{\epsilon_c(\rho)}{\gamma} - 1)}$$

β = 0.066725, $\gamma = \frac{(1-\ln 2)}{\pi^2}\gamma$, $a_0 = \frac{\hbar}{m^2}$, and the dimensionless gradient is $=\frac{|\nabla\rho|}{2K_{TF}\rho}$, where $K_{TF} = \sqrt{12/\pi}\Big/\sqrt{r_s}$ is known as the Thomas-Fermi screening wavelength and rs is defined as the local Seitz radius. The PBE-GGA functional has been extremely influential, both for performing actual calculations and as the basis for functionals involving higher derivatives and exact exchange [65]. It has been used in all studies of this thesis, and it gives a good agreement with experiment [66 – 68].

2.6. SIESTA

SIESTA is an acronym derived from the *Spanish Initiative for Electronic Simulations with Thousands of Atoms* [39] is both a method and computer program implementation, to perform electronic structure calculations and *ab initio* molecular dynamics simulations of molecules and solids. One of the main characteristics of SIESTA, that it uses the standard Kohn-Sham self-consistent density functional method in the local density (LDA) and, or generalized gradient (GGA) approximations. In addition, it utilizes norm-conserving pseudopotentials in their fully nonlocal form, and a linear combination of atomic orbital basis set to achieve efficient calculations [39].

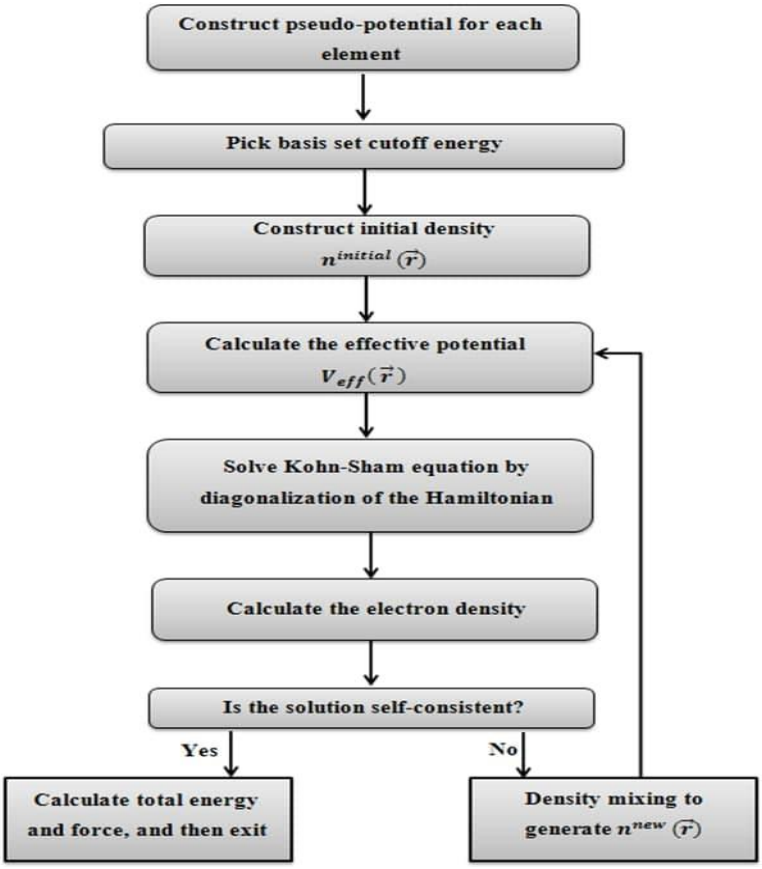

Figure 2.1. A Schematic illustration of the self-consistent DFT

In this thesis, the SIESTA code has been used to perform all DFT calculations. It is used to obtain the optimized geometries of the molecules which are the subject of this research, and a Hamiltonian describing their properties.

2.6.1. SIESTA Basis Sets

A basis set is a mathematical description of the orbital within a system used to perform the theoretical calculations. One elegant and popular choice of basis sets in periodic system calculations is the plane-wave basis set. However, one of the main reasons for applying the SIESTA code for my calculations is that it used localised basis sets (which are not implicitly periodic) and therefore can be used to construct a tight-binding Hamiltonian, this is not easy to achieve using a plane wave based code.

The type of basis set is one of the most important aspects for calculations using SIESTA. For example, to perform efficient calculations, the Hamiltonian should be sparse, and therefor SIESTA utilizes a linear combination of atomic orbital basis sets (LCAOs), which are constrained to be zero outside of a certain radius (cut-off radius), and are constructed from the orbitals of the atoms. This generates the desired sparse form for the Hamiltonian, and it reduces the overlap between basis functions, and therefore a minimal size basis set creates characteristics similar to that of the system under investigation[69].

The simplest basis set for an atom is called a single-ζ basis, which corresponds to a single basis function, $\psi_{\mathrm{nlm}}(\mathrm{r})$ per electron orbital (i.e. 1 for an *s*-orbital, 3 for a *p*-orbital, etc...). In this case each basis function consists of a product of one radial wavefunction, $\emptyset_{nl}^{1}$, and one spherical harmonic, Y_{lm}:

$$\psi_{\mathrm{nlm}}(\mathrm{r})=\emptyset_{nl}^{1}(r)\quad Y_{lm}(\varphi,\vartheta) \tag{2.23}$$

The small number of the expected basis function is one, and therefore a single-ζ basis uses single atomic orbitals as a basis function. Therefore, the radial part in equation (2.34) is found by using the Sankey method [69], because the component of the real orbital is described by an infinitely long tail, which is not suitable for a localized basis function.

This method uses a modified version of the Schrödinger equation, which is solved for an atom placed inside a spherical box, and the radial wavefunction equals zero at the cut-off radius, r_c . This restriction yields an energy shift δE within the Schrödinger equation such that eigenfunction has a node at the cut-off radius, r_c :

$$\left[-\frac{d^2}{dr^2}+\frac{l(l+1)}{2r^2}+V_{nl}^{ion}(r)\right]\emptyset_{nl}^{1}(r)=(\in_{nl}+\delta E)\varphi_{nl}^{1}(r) \tag{2.24}$$

The energy shift δE satisfies the previous constraint and the corresponding pseudopotential is $V_{nl}^{ion}(r)$.To obtain high accuracy basis sets (multiple-ζ), additional radial wavefunctions could be included for each electron orbital. The split-valence method has been used to calculate the

additional radial wavefunctions, $\emptyset_{nl}^{i}$, for $i > 1$. This involves defining a split-valence cut off for each additional wavefunction r_s^i. Thus, it is split into two piecewise functions: a polynomial below the cut-off and the former wavefunction above it:

$$\emptyset_{nl}^{i} = \begin{cases} r^1(a_{nl} - b_{nl}r^2 & r > r_s^i \\ \emptyset_{nl}^{i} & r_s^i < r < \quad r_s^{i-1} \end{cases} \qquad (2.25)$$

The additional parameters are found at the point r_s^i where the wavefunction and its derivative are assumed continuous.

The polarization of a real orbital due to the electrical field of the neighbour atoms, is taken into account to calculate the basis set function. This kind is called double-ζ polarized, which is used to achieve all calculations in this thesis. Table (2.1) shows the number of basis of orbitals for a selected number of atoms for single-ζ polarized, double-ζ and double-ζ polarized [69].

Table 2.2: Examples of the radial basis functions per atom as used within the SIESTA for different degrees of precisions[69]

Atom	SZ	SZP	DZ	DZP
H	1	4	2	5
C	4	9	8	13
S	4	9	8	13
N	4	9	8	13
O	4	9	8	13
Au	6	9	12	15

2.7. Time-Dependent Density Functional Theory (TD-DFT)

The time-dependent density functional theory (TD-DFT) extends the ground-state density functional theory by allowing for the examination of a system's excited-state features in the presence of time-dependent potentials, such as electric or magnetic fields. TD-DFT may be used to investigate the influence of fields on molecules by calculating representative excitation energies, oscillator strength, wavelength, molecular orbital character, and electronic transitions of the molecules [70]. The theoretical of TD-DFT based on the Runge-Gross theorem (R-G theorem) in 1984. The R-G theorem explained the association between the time-dependent external potential $\hat{V}_{ext}(\vec{r})$ and $\rho(\vec{r}\,,t)$ of the system. R-G theorem designated that when two external potentials $\hat{V}_{ext}(\vec{r})$ and $\widehat{V'}_{ext}(\vec{r})$ have an alteration of more than a time-dependent function, their own electron densities $\rho(\vec{r}\,,t)$ and $\rho'(\vec{r}\,,t)$ are also dissimilar [71].

Runge and Gross discussed how excited states are obtained using TD-DFT. The starting point of studying time-dependent systems is the time-dependent Schrodinger equation. The TD-DFT is straight related to the Schrodinger equation $\left[i\,\hbar\,\frac{\partial}{\partial t}\,\Psi\,(\,\vec{r}\,,t\,) = \hat{H}\,\Psi\,(\,\vec{r}\,,t\,)\right]$ where the Hamiltonian is known to be [72]:

$$\hat{H} = \hat{T} + \hat{V}_{\text{elec.elec}} + \hat{V}_{\text{ext.}}(\vec{r}\,) \qquad (2.26)$$

Here, $\hat{H}$ consists of the kinetic energy operator $\hat{T}$ electron-electron repulsion $\hat{V}_{\text{elec.elec}}$ (Coulomb operator) and the external potential $\hat{V}_{\text{ext.}}(\vec{r})$. Where $\hat{V}_{\text{ext.}}$ $(\vec{r})$ is given in the following operators:

$$\hat{V}_{\text{ext.}}(\vec{r})=\sum_{i=1}^{N} V_{ext.}\ (\vec{r_i}\ ) \tag{2.27}$$

The densities of the system rise from a fixed first state $\Psi\ (\ t_o) = \Psi\ (\ 0\ )$. The first state, $\Psi\ (\ 0)$ is arbitrary, it must not be the ground-state or some other eigen state of the first potential $\hat{V}\text{ext.}\ (\vec{r}) = \hat{V_o}\ (\vec{r})$. The R-G theorem indicates that there exists an one-to-one correspondence between the time-dependent external potential $\hat{V}\text{ext.}\ (\vec{r})$, and the time-dependent electron density $\rho(\vec{r}\ , t)$, for systems developing from a fixed first many-body state. Translation to it, the density determines the external potential, and next helps in obtaining the time-dependent many-body wave functions [73,74]. As this wave-function controls all observables of the system as an important, the saying point is that all observables are functionals of $\rho(\vec{r}\ , t)$. The statement of the theorem is the "densities $\rho(\vec{r}\ , t)$ and $\rho'(\vec{r}\ , t)$ evolving from the same initial state $\Psi(0)$ under the effect of two potentials $\hat{V}_{\text{ext.}}\ (\vec{r})$ and $\widehat{V'}_{ext}(\vec{r})$ are always different provided that the potentials differ by additional than a chastely time-dependent function [70,72]:

$$\hat{V}_{\text{ext.}}\ (\vec{r}\ , t) = \widehat{V'}_{ext}(\ \vec{r}\ , t\ ) + C(t) \tag{2.28}$$

Where the $C(t)$ allows increase to wave functions that are different only by a phase factor $e^{-iC(t)}$, therefore, the same electronic density is stable. R-G theorem states that the density is a functional of the external potential and of the first wave function on the space of potentials differing by more than the addition of C(t).

2.8. Gaussian Program 09 (G09)

Gaussian is a general-purpose computational chemistry software program that was first released as Gaussian 70 in 1970 by John Pople and his research group at Carnegie Mellon University. It has been constantly updated since then. The term comes from Pople's use of Gaussian orbitals to speed up molecule electronic structure computations rather than Slater-type orbitals [73,72]. A decision is taken to increase performance on the restricted processing capabilities of the time's computer hardware for Hartree–Fock computations. Gaussian 16 is the most recent version of the software [75]. Initially accessible through the Quantum Chemistry Program Exchange, it was later licensed out of Carnegie Mellon University and has been developed and licensed by Gaussian since 1987.

Gaussian can predict molecular energies and structures, transition state energies and structures, vibrational frequencies, IR and Raman spectra, thermochemical properties, bond and reaction energies, reaction pathways, molecular orbitals, atomic charges, vibrational circular dichroism intensities,

electron affinities and ionization potentials, polarizabilities and hyperpolarizabilities, and electrostatic potentials and electron densities [76].

2.9. The Landauer Formula

The Landauer formula [77, 78] was first suggested by Rolf Landauer in 1957 [79] for two terminals. To illustrate the formula, consider a scattering region connected to two electrodes (leads) as sketched in Figure 2.1. The leads are assumed to be ballistic conductors, i.e. conductors with no scattering and thus the transmission probability equals one [80]. Each lead, in turn, is coupled to a reservoir where all inelastic processes take place.Suppose that the chemical potentials of the reservoirs on the left and right hand sides are , respectively, and let the temperature be equal to zero (T = 0)

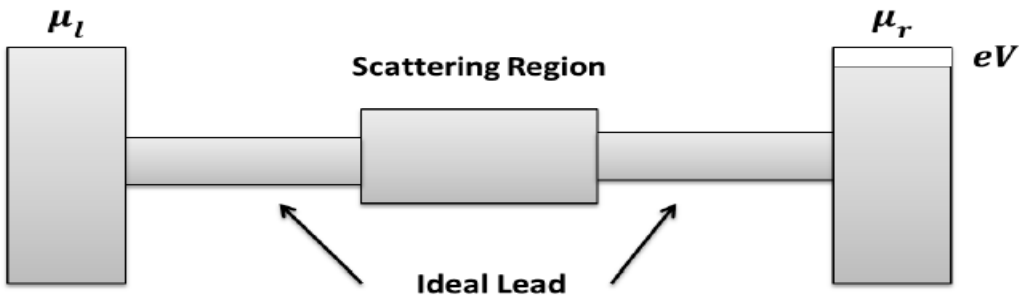

Figure 2.3: *Schematic view of a 1-D scattering region connected to two reservoirs with different chemical potentials μ_L and μ_R via ideal leads*

Consider the case of a 1-dimensional system. When the scattering region is an ideal 1-dimensional lead, so that the two reservoirs are connected by a perfect 1-

d lead with no scattering, the current through this system, which flows due to the chemical potential difference between the reservoirs is,

$$I = (-e)v\ \frac{\partial n}{\partial E}(\mu_l - \mu_r) \quad (2.29)$$

Here v is the group velocity, e is the electronic charge and $\frac{\partial n}{\partial E}$ is the density of states per unit length of the electrons which is given by $\frac{\partial n}{\partial E} = \frac{1}{\pi\hbar v}$ It is worth mentioning that the Landauer formula describes the linear response conductance, hence it only holds for small bias voltages, $\delta V \rightarrow 0$ Thus,

$$I = \frac{-2e}{\hbar}\ \ (\mu_l - \mu_r) \quad (2.30)$$

In the presence of the scatter, these electrons have a transmission probability T to traverse the scattering region, therefore, the current flow is [80]:

$$I = \frac{-2e}{\hbar}\ T\ \ (\mu_l - \mu_r) \quad (2.31)$$

Since the chemical potentials difference between the reservoirs is given by ,$-eV = (\mu_l - \mu_r)$, the conductance between the two terminals is obtained as:

$$G = \frac{I}{V} = \frac{2e^2}{\hbar}\ \mathrm{T} = G_0\ T \quad (2.32)$$

Where $G = \frac{2e^2}{\hbar}$. This relation is called Landauer formula for a one-dimensional system [77, 78]. For a perfect conductor where $T = 1$, the Landauer formula becomes:

$$G = G_0 \approx 12.9(k\Omega)^{-1} \quad (2.33)$$

Where G_0, is the conductance quantum. At a finite temperature the Landauer formula (2.46) is transformed into the more general formula for the current [79]:

$$I = \frac{2e}{h}\int T(E)[f(E-\mu_l) - f(E-\mu_R)]dE \qquad (2.34)$$

Where f is the Fermi-Dirac distribution $f(E-\mu) = 1/(1+e^{\frac{E-\mu}{k_BT}})$ related to the chemical potential μ , T is temperature and k_B is Boltzmann‘s constant. In the case of the linear response regime (i.e. at low bias eV), the Fermi-Dirac functions in eq. (2.49) can be Taylor expanded around the Fermi energy [80] resulting in:

$$I = \frac{2e^2V}{h}\int_{-\infty}^{\infty}\left[-\frac{\partial f(E)}{\partial(E)}\right]\ T\ (E)\ \ dE \qquad (2.35)$$

Last equation shows that when the voltage is small, the current is linearly proportional to the voltage, and then we can write:

$$I\ = G\ V \qquad (2.36)$$

Where G is the conductance of the two terminals device. Thus:

$$G = G_0\int_{-\infty}^{\infty}\left[-\frac{\partial f(E)}{\partial(E)}\right]\ T\ (E)\ \ dE \qquad (2.37)$$

As mentioned above, the current in equation (3.51) is linearly proportional to the voltage and because of this linearity, this system of transport is called linear response regime.

2.10. Green’s Functions

Green‘s function (GF) is a useful tool for studying the properties of nano-scale structures because it can be used to express all of the observable properties

of the system of interest [81]. In this section I will first discuss how to construct the Green's function for some separate lattices. Then we will briefly discuss how to connect the Green's functions of these separable lattices together to construct the Green's function of the whole system using Dyson equation.

2.11. GOLLUM Program

Charge, spin, and electronic contributions to the thermal transport properties of multi-terminal junctions are calculated using the GOLLUM program. GOLLUM has a simpler structure, is faster, and consumes less memory since it is based on equilibrium transport theory.

The software has been developed for ease of use, and it represents a significant step forward in the implementation of ab-initio multi-scale simulations of traditional and more advanced transports functions. GOLLUM's simplified interface allows it to read model tight bound Hamiltonian's. Furthermore, GOLLUM is designed to readily interact with any DFT code that employs a localized basis set. It now reads data from all of the most recent public versions of the code SIESTA [82].

GOLLUM can model these materials' connections using parameterized tight-binding Hamiltonians [83,84] or DFT .

DFT fails to account for the significant electronic correlation effects found in many Nano-scale electrical connections. As a result, GOLLUM provides a number of methods for dealing with high correlations[85,86].

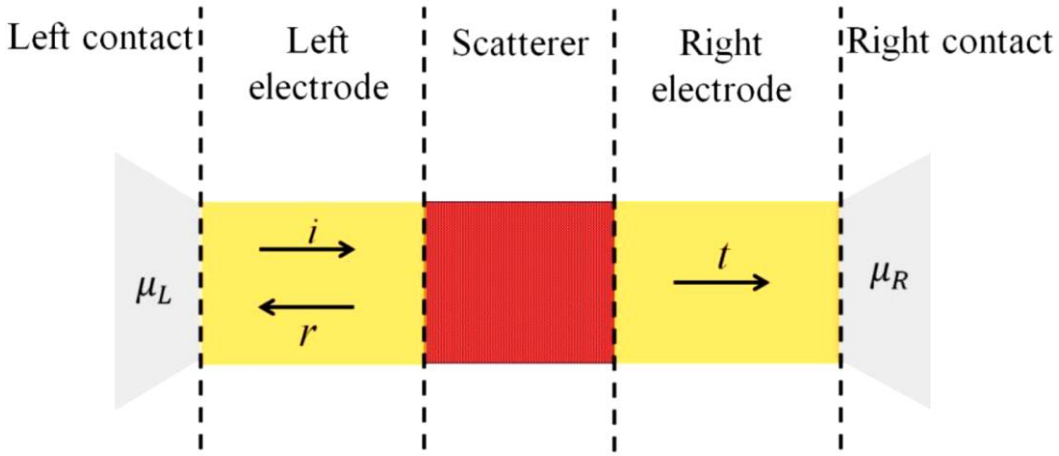

Figure 2.4:"*Illustrates a mesoscopic scatterer connected to contacts by ballistic leads. The μL and μR represent the chemical potential in the contacts. When an incident wave packet hits the scatterer from the left then it will be transmitted with probability* $T = tt*$ *and reflected with probability* $R = rr*$ *where,* t, $t*$, r *and* $r*$ *represent the transmission and the reflection amplitudes from the left to the right and vice versa. Charge conservation requires* $T + R = 1$.

Chapter Three

Results and Discussion

3.1. Introduction

The idea of building electronic devices using single molecules as active components was first proposed by Aviram and Ratner in 1974. Indeed, molecules are of great interest for application in electronic devices because of their small size, recognition properties, unique ability to self-assemble (specific/highly selective interactions) and versatility of their chemical modification and/or customization. Thus, the ability to measure and control charge transport across the metal–molecule–metal junction is of considerable fundamental interest and represents a key step towards the development of single-molecule electronic devices.

A critical issue in all these experimental and theoretical studies is the formation of a reliable electrical contact between the target molecules and the macroscopic electrodes surface. Therefore, it is very important to understand the effect of the anchoring group on the electron transport through the molecular junction.

In this context, this study will discuss some of the important results on the anchoring group effect on the electronic, electric, thermoelectric and spectral properties of single molecular junction.

3.2. Structural Properties

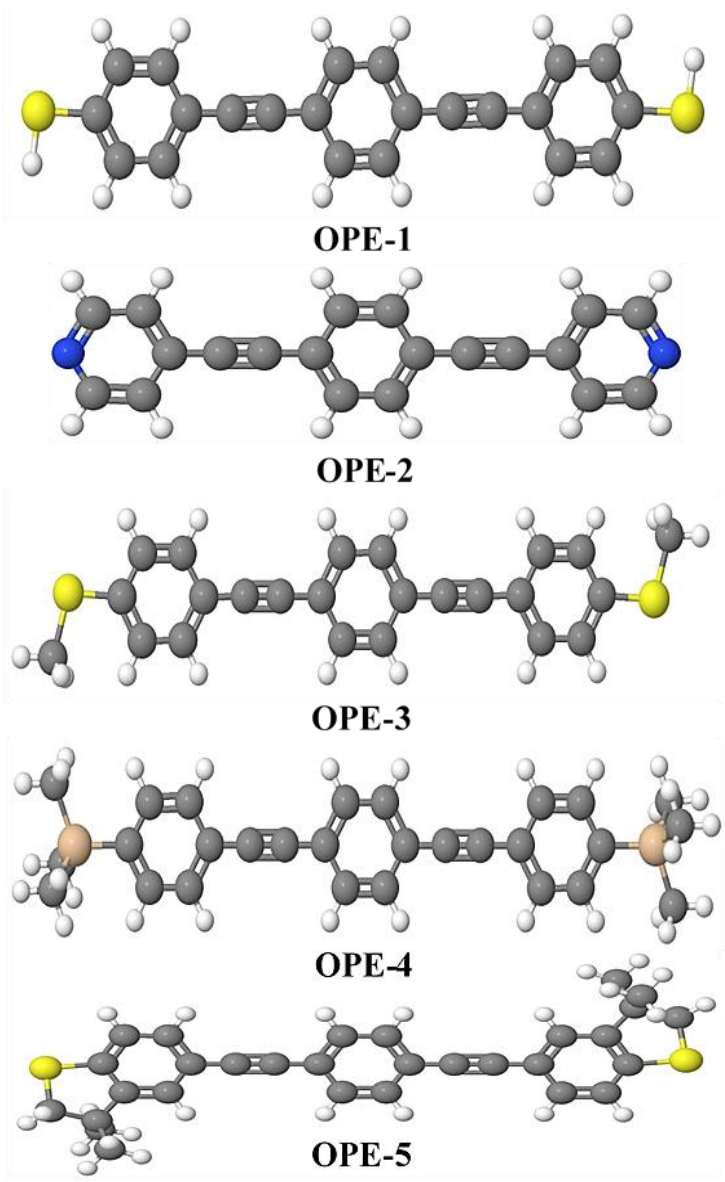

Figure 3.1. The relaxed geometries of all molecules.

The oligo(phenyleneethynylene) (OPE) molecules are shown in Figure 3.1, with five different anchor groups. The first molecule (OPE-1) posses thiol (SH) contact groups, while the second molecule (OPE-2) have pyridine (PY) anchor groups. The third, fourth and fivth molecules (OPE-3, OPE-4 and OPE-5) have methyl sulfide (SMe), tetramethylsilane (TMS) and dibenzothiophene (DBT) respectively.

The choice of anchoring group can determine the nature of charge transport in the system to be either p-type (HOMO-dominated) or n-type (LUMO-dominated) by the rearrangement of front molecular orbitals (FMOs). In this way, anchoring groups can be discriminated by their electrode-coupling induced charge transfer properties.

Table 3.1. The structural aspect of all molecules. L is the molecule length, D (Au…Au), is the molecular length. X is the bond length. Z (D – 0.25), is the theoretical electrodes separation. C–N is the carbon-nitrogen single bond. C–S is the carbon-sulfur single bond. C–Si is the carbon-silicon single bond. ∠ is the angle between carbon atom, anchor atom (N or S or Si) and gold atom for contact group.

Molecule	L (nm)	D (nm)	X (nm)	Z (nm)	C–N (nm)	C–S (nm)	C–Si (nm)	∠ (°)	Anchor groups
OPE-1	2.031	2.474	0.245	2.224	-	0.182	-	52°	SH
OPE-2	1.663	2.111	1.861	2.905	0.135	-	-	160°	PY
OPE-3	2.031	2.474	0.245	2.224	-	0.182	-	52°	SMe
OPE-4	2.052	2.576	0.285	2.326	-	-	0.192	160°	TMS
OPE-5	2.023	2.474	0.245	2.224	-	0.182	-	52°	DBT

From figures 3.1, 3.2 and Table 3.1, it can be observed that there are noticeable differences in the structural aspects of these molecules, as the lengths of the molecules are varied from 1.663 nm for molecule OPE-2 to 2.052 nm for molecule (OPE-4), as well as the lengths of the bonds between the bonding atoms of the anchor groups. In addition to the theoretical molecular length is also varied. Furthermore, there are various angles

between carbon atom, anchor atom (N or S or Si) and gold atom for contact groups. Undoubtedly, these structural aspects will affect the junction formation probability and all other properties (electronic, electric, thermoelectric and spectral) of these molecules.

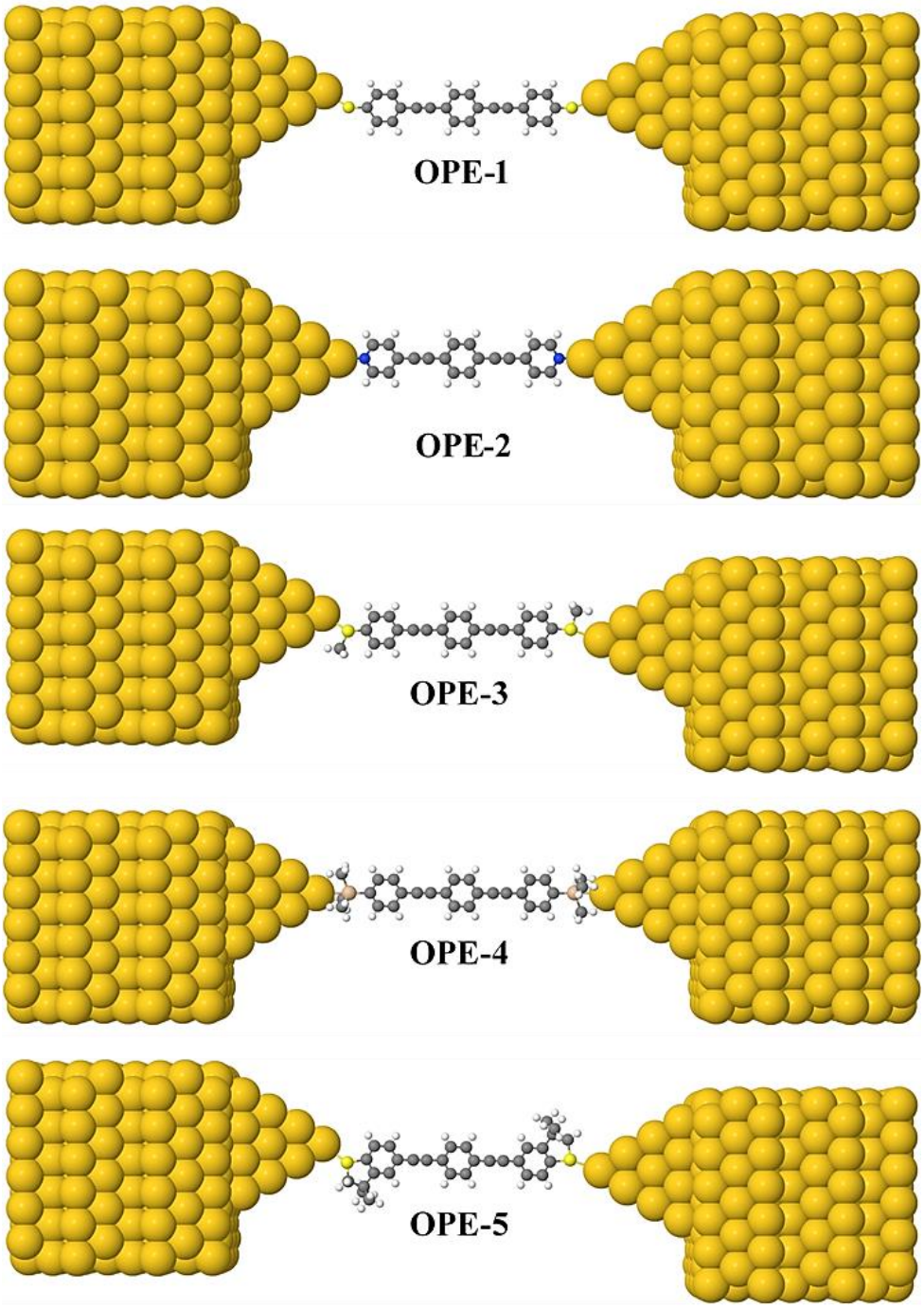

Figure 3.2. The relaxed geometries of all molecular junctions.

Figure 3.2 shows that the molecular junction was created by attaching the molecule to 35-atom pyramidal gold electrodes with base layers consisting of 6×6 atoms and a layer spacing of 0.235 nm. Then the constructed structure was geometrically relaxed, while the base layers of the pyramids were held fixed. These base layers were then repeated to yield infinitely-long current-carrying gold leads. Finally, it can be observed that this kind of molecules is rigid, since all molecules kept their backbone without bending or twisting, and this makes these molecules an excellent candidate for optoelectronics field, components and applications.

The optimized molecular junction geometries conform well to a description of the SH, SMe and BDT contacted compounds forming an angle of 52º contact between anchor groups and the undercoordinated gold atoms of the gold electrodes. Also, it shows that PY and TMS contact groups create an angle of 160°. As expected, figure 3.2, and table 3.1 show that all contacted compounds are oriented normal to the idealized pyramidal gold electrode surface within the molecular junction, and produce an ideal junction formation probability.

3.3. Electronic Properties

Designing highly conductive single-molecule junctions is critical for their potential application to components of small electronic devices. Charge transport through a single-molecule junction can be explained using the tunneling barrier model.

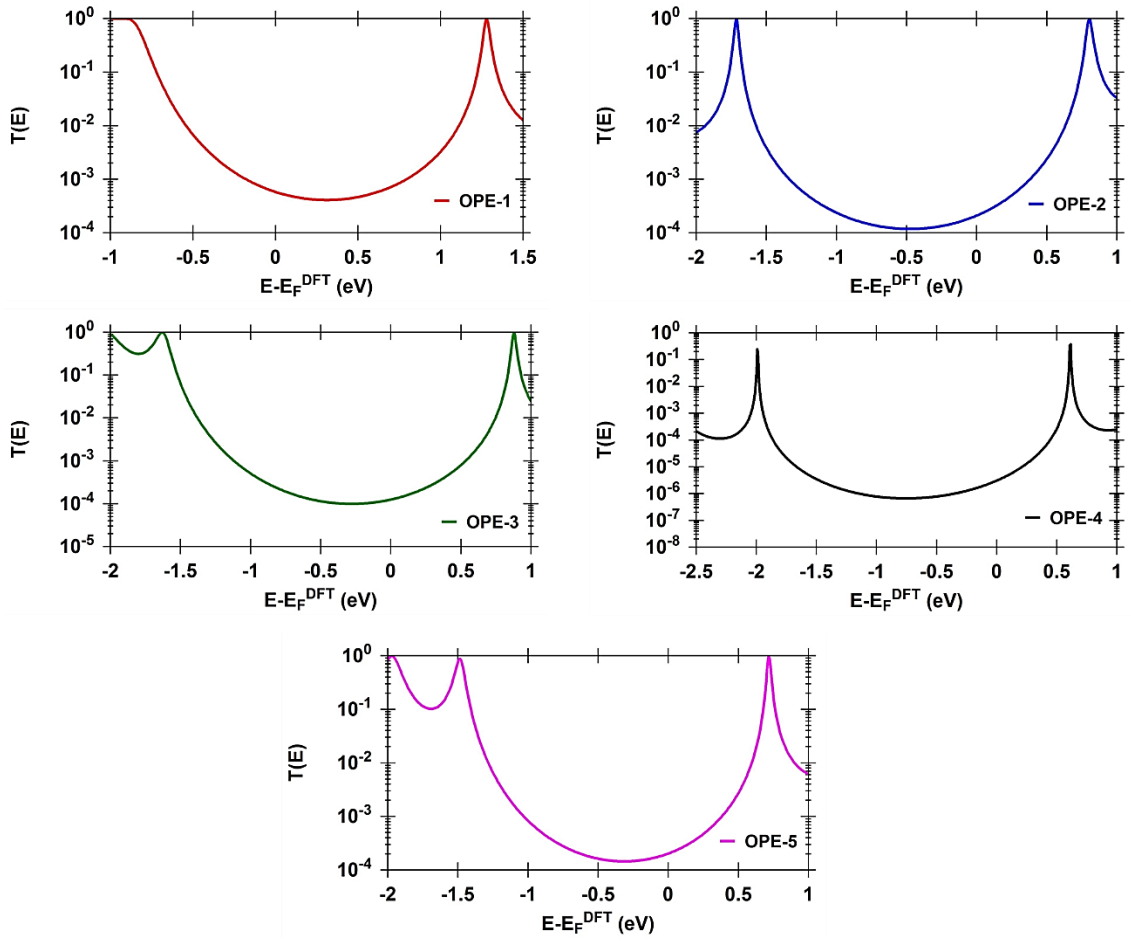

Figure 3.3. Represents the transmission coefficient T(E) as a function of electrons energy of all molecules.

The transmission coefficient T(E) is a property of the whole system comprising the leads, the molecule and the contact between the leads and the molecule. Nevertheless, if the contact to the electrodes is weak, then a graph

of T(E) versus E will reflect the energy-level structure of the isolated molecule. In particular if the isolated molecule has energy levels E_Γ, (where Γ represents the quantum numbers labelling the energy levels), then T(E) will possess a series of peaks (ie resonances) located at energies in the vicinity of the levels E_Γ. In general, the transmission coefficient T(E) describing the propagation of electrons of energy E from the left to the right electrode. In this thesis, the transmission coefficient have been calculated by first obtaining the corresponding Hamiltonian and overlap matrices using SIESTA and then using the GOLLUM code. Figure 3.3 shows that OPE-1 introduces a high value of transmission coefficient (5.8×10^{-4}), while the lowest value of the transmission (3.12×10^{-6}) is presented by molecule (OPE-4). On the other hand, it can be seen that the transport mechanism for molecule OPE-1 is a HOMO-dominated transport, while for other molecules is an LUMO-dominated mechanism.

In general, the transmission coefficient value of all molecules is high, and that can understand in terms of the quantum interference is a constructive interference and there is no a destructive interference signature within the gap. The order of the transmission is $T(E)_{OPE-1} > T(E)_{OPE-2} > T(E)_{OPE-5} > T(E)_{OPE-3} > T(E)_{OPE-4}$.

This trend can be attributed to the uniformity of the binding geometries and a decrease in binding energy and/or junction stability.

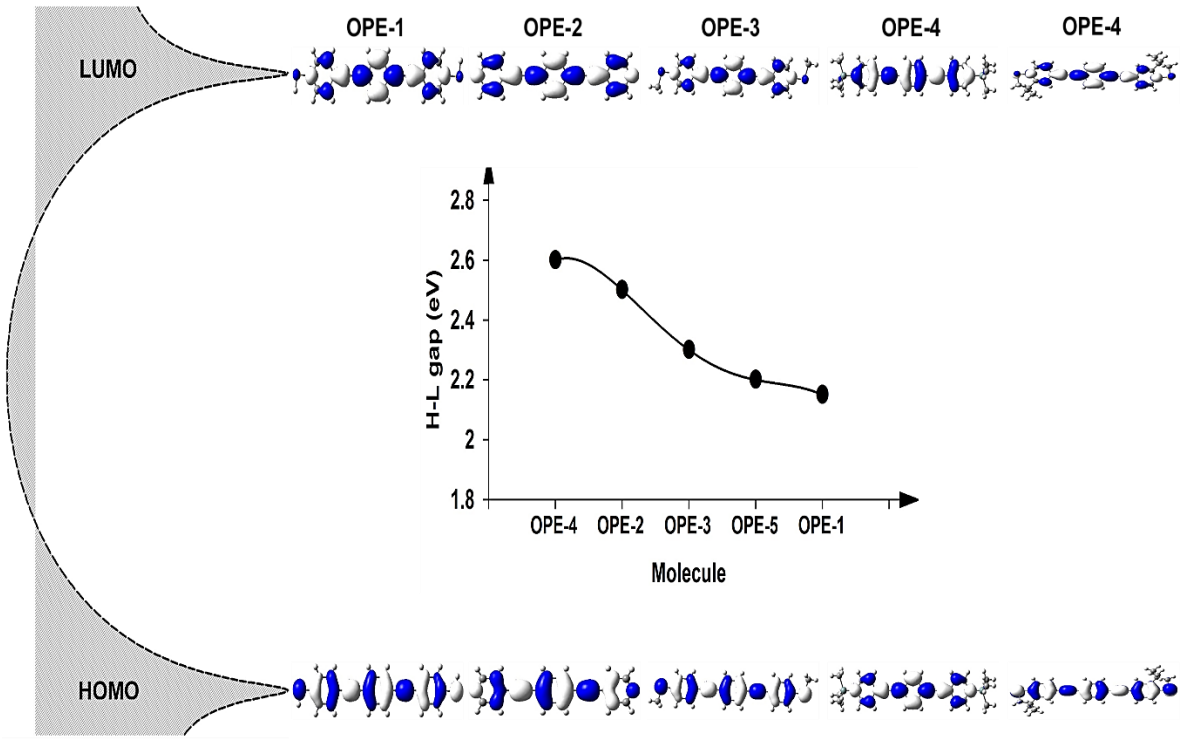

Figure 3.4. The iso-surfaces (±0.02 (e/bohr^3)$^{1/2}$) of the HOMOs and LUMOs for all molecules. The insert figure shows the trend of HOMO-LUMO gap of all molecules.

These results provide a convenient point to commence discussion and a basis for comparison between the highest occupied and lowest unoccupied molecular orbitals HOMO and LUMO, respectively. Unsurprisingly, the lowest and highest energy structures features arrangement the electronic structure with the frontier orbitals distributed almost evenly across the molecular backbone, making a linear, p-type conjugated pathway between the two anchor atoms. On the other hand, the lowest unoccupied molecular orbitals are localized on the (C≡C) bonds and shown more contribution than that of the highest occupied molecular orbitals, which are concentrated on the (C=C) bonds. It is worth to mention that the weight of the LUMO on the

PY, TMS, DBT and SMe anchor groups is noticeable, and higher than that of the HOMO. These results reflect two points. The first one is the transport mechanism of the charge carriers could be the LUMO-dominate transport mechanism for molecules OPE-2, OPE-3, OPE-4 and OPE-5, while the weight of HOMO is the hieghest on SH anchor groups for molecule OPE-1. Hence, the transport mechanism through this structure is HOMO-dominated transport, which consistent with the transmission coefficient results. The second point is the molecular junction formation probability of all molecules is too high, as well as the stability of the junction.

Table 3.2. T(E) is the transmission coefficient; H-L is HOMO-LUMO gap energy; B.E. is the binding energy; Γ is the number of transfer electrons from anchor atoms to electrodes.

Molecule	T(E)	H-L gap (eV)	B.E. (eV)	Γ
OPE-1	5.87×10^{-4}	2.15	0.67	7.13
OPE-2	2.13×10^{-4}	2.5	0.52	6.78
OPE-3	1.26×10^{-4}	2.3	0.45	6.12
OPE-4	4.12×10^{-6}	2.6	0.23	2.18
OPE-5	2.05×10^{-4}	2.2	0.41	6.03

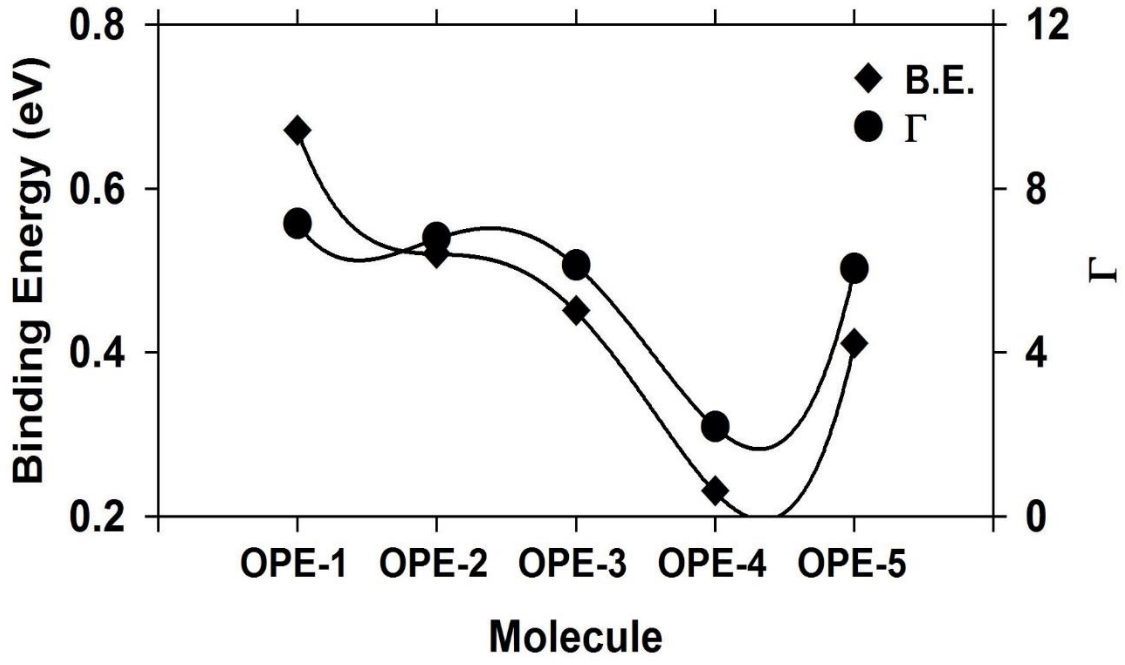

Figure 3.5. Represents the binding energy (B.E.), and the number of transfer electrons (Γ) from anchor atoms to electrodes of all molecules.

The binding energy (B.E.) is the lowest energy required to make the system stable at an "equilibrium interaction distance". To obtain an ideal arrangement of the molecule–electrodes contact, the binding energy calculations with a generalized gradient approximation (PBE functional), double-zeta polarized basis set, 0.01 eV/A force tolerance and a real-space grid defined with a plan wave cut-off energy of 250 Ry, were performed using the Counterpoise method to overcome basis set superposition error correction (BSSEC). On the other hand, it may be worth mentioning, that when a molecular wavefunction is obtained by quantum mechanical calculations, one wishes to extract useful chemical-physics information from it or to interpret it in terms of more intuitive chemical notions. For a molecular wavefunction in the a linear combination of atomic orbitals

Molecular orbitals (LCAOMO) approximation, the most frequently used method to calculate the number of transfer electrons (Γ) from anchor atoms to electrodes is Mulliken population analysis.

Figure 3.5 shows that the hieghest binding energy is presented from molecule OPE-1, and this not only support the high value of transmission coefficient of this molecule as shown in Figure 3.3, but also it interprets the highest value of transfer electrons from this molecule to electrodes. Whereas, the lowest binding energy and Γ are introduced by molecule OPE-4.

These results prove the fact that there is a close relationship between the binding energy and the electronic transition, as the type of anchor group will determine the value of the binding energy, which in turn will determine the probability of the molecular junction formation, which in turn will determine the value of the transmission coefficient. In light of these results, it can be concluded that choosing the anchor group will greatly help researchers in improving the various properties of electronic devices based on single molecules, as well as in determining the appropriate application of those molecules.

3.4. Spectral Properties

In spectroscopy, oscillator strength is a dimensionless quantity that expresses the probability of absorption or emission of electromagnetic radiation in transitions between energy levels of an atom or molecule. For example, if an emissive state has a small oscillator strength, nonradiative decay will outpace radiative decay. Conversely, "bright" transitions will have large oscillator strengths.

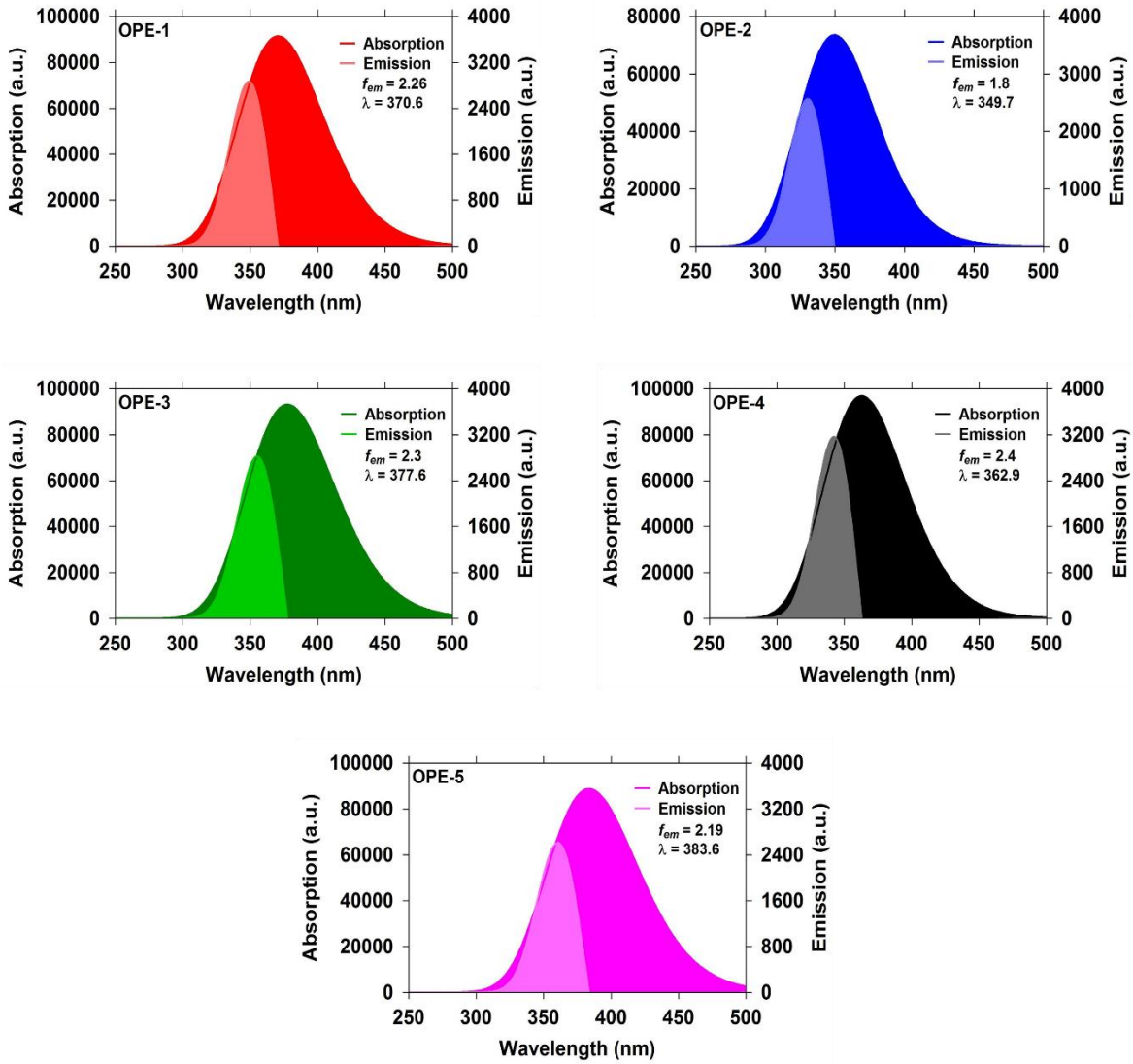

Figure 3.6. Represents the absorption, emission and emission oscillator strength (f_{em})of all molecules.

The oscillator strength can be thought of as the ratio between the quantum mechanical transition rate and the classical absorption/emission rate of a single electron oscillator with the same frequency as the transition.

Figure 3.6 presents the absorption and emission results for all the molecules under study in this thesis. Initially, it can be noticed that the emission intensity of the molecule (OPE-4), which characterized by TMS anchor groups is higher than those with other contact groups. Since its value was 3165 a.u. While, the emission intensity values for molecules with SH, PY, SMe and DBT are 2868 a.u., 2568 a.u., 2823 a.u., 2610 a.u. respectively. The second important result is exhibited in figures 3.6, 3.5 and tables 3.2, 3.3 which is the emission oscillator strength (f_{em}), and it relationship with the electrons transfer and transport connect groups. The molecule OPE-4 with TMS anchor gropus produces the highest f_{em} (2.4), while the molecule (OPE-2) with PY contact groups shows the lowest f_{em} (1.8). In addition, it could be observed that the maximum wavelength (λ_{max}) for all molecules lies in the UV region, and there is also a fluctuation from 349.7 nm for OPE-2 to 383.6 nm for OPE-5. Based on these results, we can conclude that changing the anchor groups not only affects the intensity of the absorption, but also leads to a displacement in wavelengths.

The order of emission and absorption intensities and the emission oscillator strength is OPE-4 > OPE-3 > OPE-1 > OPE-5 > OPE-2. These results can

formulate for us a promising theoretical strategy for choosing the structures and materials that can serve as an active laser medium. Since, the emission cross section (σ_{em}) of a laser transition is consider an important parameter, because it can impact the accomplishment of laser in terms of the threshold energy, output energy, maximum gain, etc.. In other words, the high value of emission cross section (σ_{em}) leads to high gain laser, and since it is a direct proportion between the emission cross section and the emission oscillator strength. Therefore, our theoretical strategy to enhance the emission via change the transport connect groups of molecules can be a powerful way to develop the laser technique.

Table 3.3. The emission and absorption intensities, and the emission oscillator strength (f_{em}).

Molecule	f_{em}	Absorption (a.u.)	Emission (a.u.)
OPE-1	2.25	91372.9	2868
OPE-2	1.8	73532.3	2568
OPE-3	2.3	93160.5	2823
OPE-4	2.4	96874.4	3165
OPE-5	2.19	88747.3	2610

3.5. Electrical Properties

The electrical properties of an open system are influenced by both the properties of the isolated molecule and the contact between the molecule and electrodes. Therefore, electrical conductance calculations need to include both features to understand the scattering process of an electron between the two electrodes. In this thesis, the electrical conductance have been calculated by first obtaining the corresponding Hamiltonian and overlap matrices using SIESTA and then using the GOLLUM code.

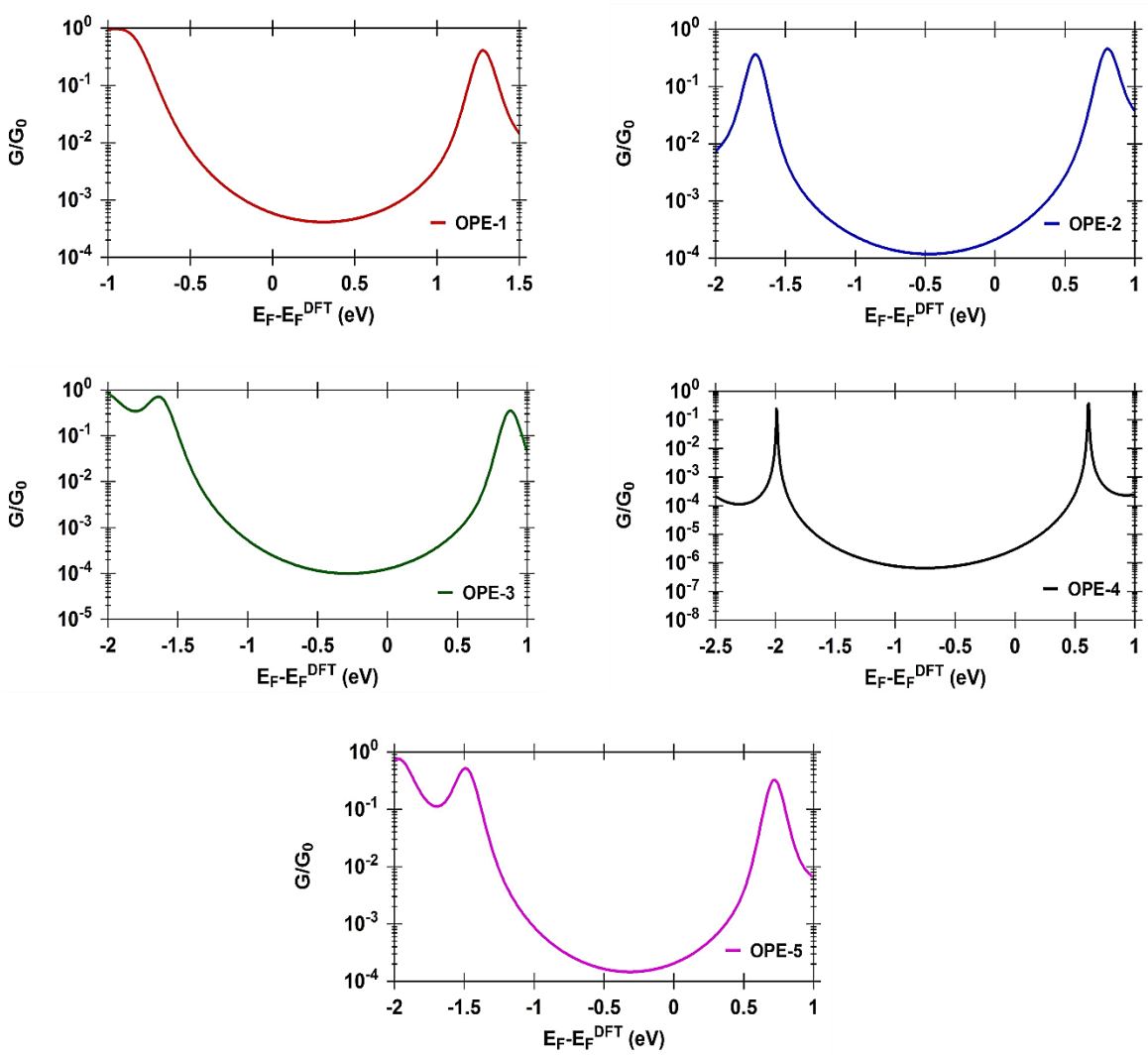

Figure 3.7. Represents the electrical conductance (G/G_0) as a function of Fermi energy for all molecules.

The electrical conductance as a function of Fermi energy is reported in Figure 3.7. However, it is interesting the conductance of molecule OPE-4 is the smallest (two orders of magnitude smaller than that of OPE-1). Such behavior can be justified as a consequence of quantum interference of the molecular orbitals, where the variation of interference conditions is due to the presence of anchor groups which involve the silicon atoms. Although, the strong chemical bond is realized between the sulfur atoms and gold pads for molecules OPE-3 and OPE-5 the conductance of these molecules are peaked in the midel of HOMO-LUMO gap near to the LUMO. This reflects the localized character of the chemical bond, which means that the sulfur atoms partially insulate the delocalized pi-electron states which are mainly involved into the conduction process. The presence of carbon and hydrogen atoms in the anchor groups of these molecules leads to a weak-coupling case in which conducting channels are electrically isolated from metallic electrodes via potential barriers as shown in Figure 3.8 as an example of electronic transmission channels overlap.

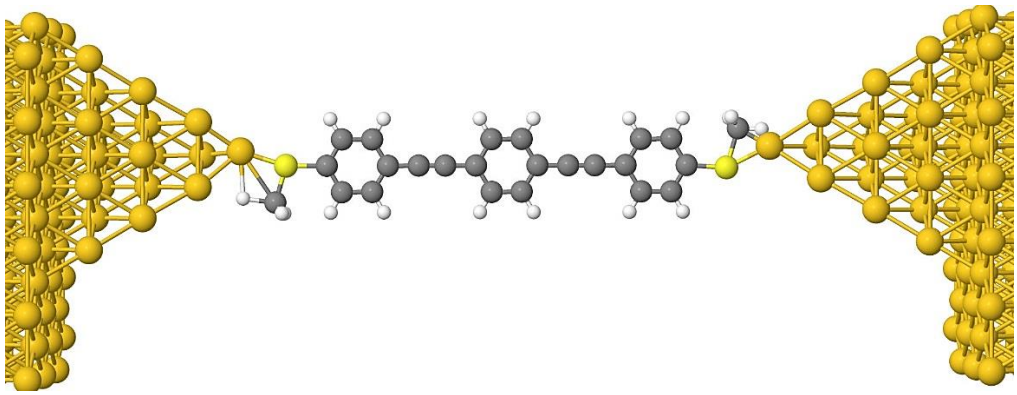

Figure 3.8. Represents an example of electronic transmission channels overlap.

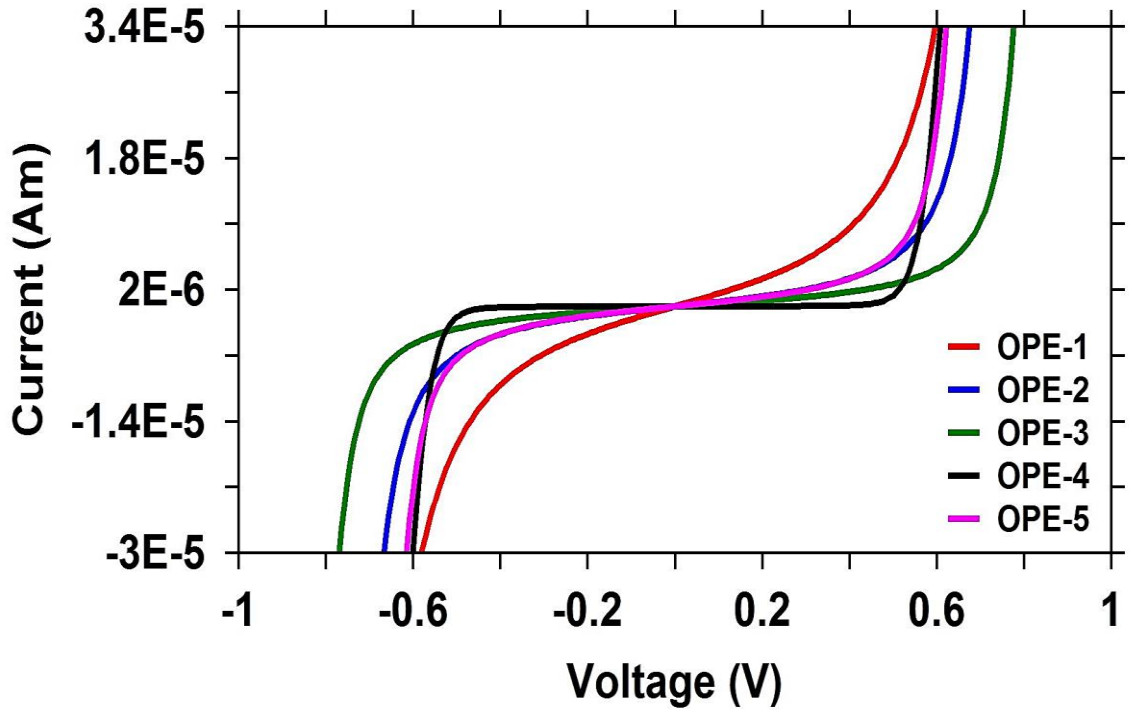

Figure 3.9. The current-voltage characteristics of all molecular junctions.

Primarily, figure 3.9 shows molecular junctions with current-voltage (I–V) characteristics curves which pass through the second quadrant, which means that they are active components, power sources, which can produce electric power. In addition, these results show threshold voltage (V_{th}), which is one of the most important physical parameters to determine and predicate the appropriate application, such as a field-effect transistor (FET), diodes and light emitting diodes. Threshold voltage is defined as the gate voltage at which the device starts to turn on. The accurate modeling of threshold voltage is important to predict correct circuit behavior from a circuit simulator. Figure 3.9 predicates that the V_{th} of these molecular junction is between 0.43 V to 0.68 V as shown in Table 3.4, which makes them perfect candidates for electronic and optoelectronic applications.

The analyzing the *I–V* curves of Figure 3.9 within the framework of the tunneling transport model, it could identify those contacts that are indeed formed by a single molecule. Under these conditions also symmetric coupling situations can be achieved that can be explained by physisorption of the end-groups to the electrodes. This study demonstrated that the change of the conductance is mainly achieved by tuning the coupling of the molecular orbital of anchor groups to the metal electrode while the dominant transport level E_0 remains mainly constant. In addition, it could be conclude that the molecules favoured physisorption, since both the coupling and the energy of the frontier orbital can be tuned. These findings are important for the further improvement of photochromic molecules in future molecular electronic devices. Furthermore, these results found rather broad distributions of conductance values in states. Finally, The analysis based on the assumption that the current is carried by a single dominating molecular orbital, reveals distinct differences between states.

Table 3.4. The electrical conductance (G/G_0), and the threshold voltage (V_{th}).

Molecule	G/G_0	V_{th} (V)
OPE-1	0.59×10^{-3}	0.43
OPE-2	0.21×10^{-3}	0.61
OPE-3	0.13×10^{-3}	0.68
OPE-4	0.31×10^{-5}	0.54
OPE-5	0.2×10^{-3}	0.56

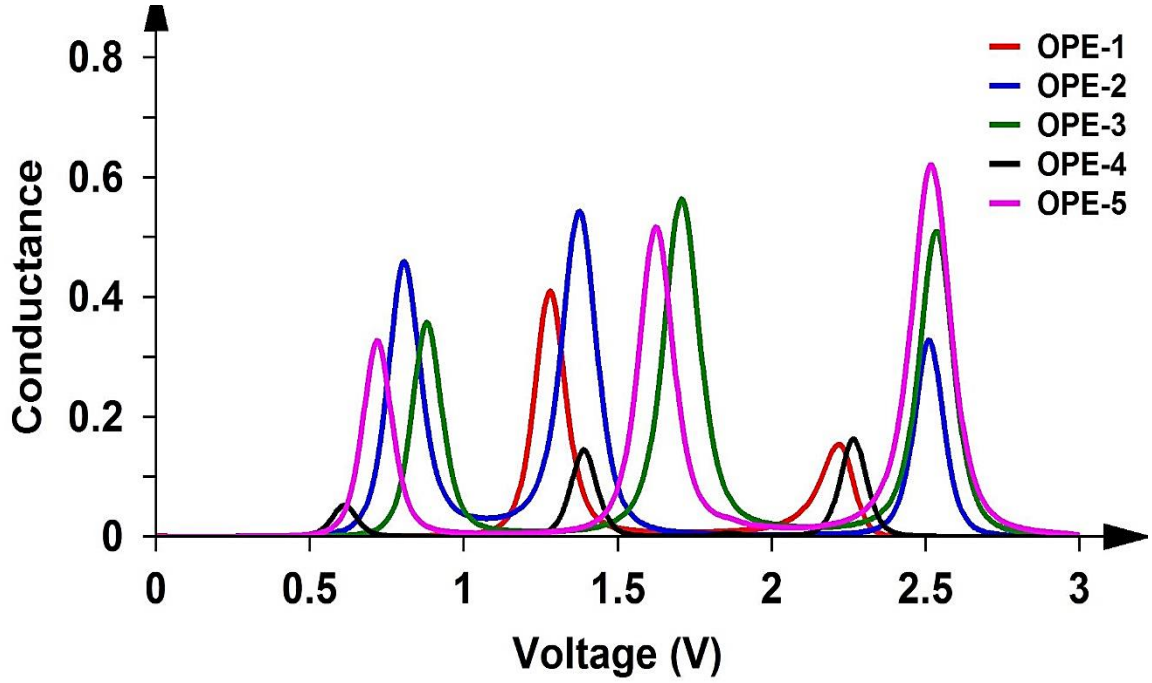

Figure 3.10. Represents the electrical conductance (G/G_0) as a function of the applied voltage for all molecules.

According to the results presented in Figure 3.10, important features are reported in the following notes: (a) The conductance-voltage characteristic shows very sharp resonant peaks at the position of the resonance level of the molecule. (b) With increasing of the electronvibration interaction strength, the conductance-voltage characteristic exhibits a peak at the inelastic threshold voltage. This change in the conductance due to the additional broadening associated with energy dissipation to the vibrational excitation. (c) When the molecular bridge-leads coupling strength increases, the width of these resonances gets more enhancement substantially, where the plateau heights depend on the molecular bridge-leads coupling parameters. (d) The resonant peak of the conductance-voltage characteristic becomes wider and lower with increasing the junction temperature. (e) None difference in the

spectra of the conductance with increasing of the vibrational mode energy. Finally, it is observed that the molecular bridge-leads coupling strengths and the junction temperature have a significant role in the determination of electronic transport characteristics (the electron conduction) through a single molecule junction in the presence of electron-vibration coupling.

3.6. Thermoelectric Properties

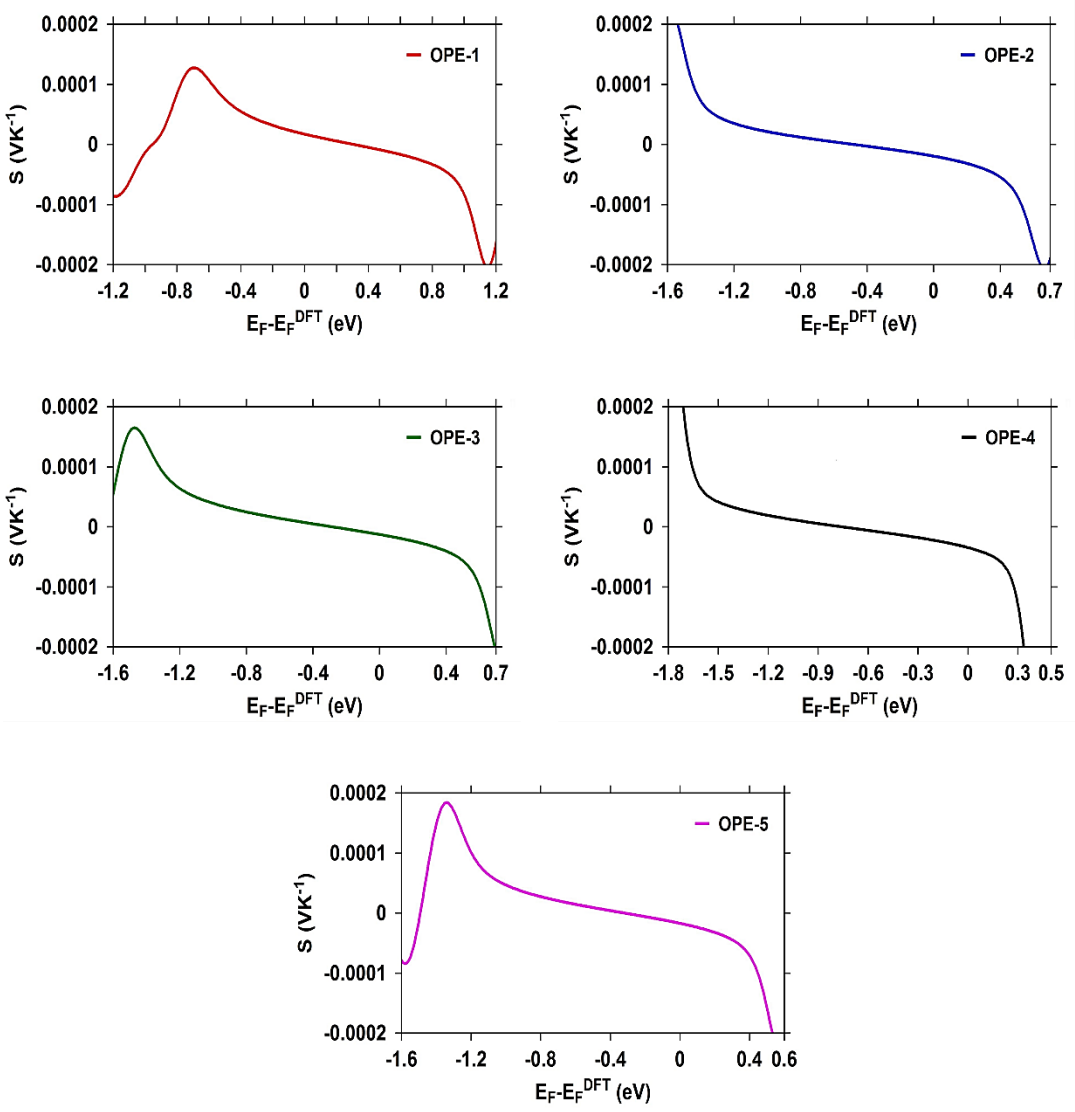

Figure 3.11. Represents the thermopower (S) as a function of Fermi energy for all molecules.

The computed values of the thermopower reflect some of facts. Firstly, it demonstrated that we can determine the conductance and thermoelectric current concurrently through single-molecule junctions. The thermoelectric currents are used to determine a Seebeck coefficient for each junction. We find that thiol-terminated molecular junctions have a positive Seebeck coefficient in agreement with calculations that show that the HOMO is the molecular resonance that is closest to E_F. In contrast, SMe, DBT, PY and TMS-terminated molecular junctions have a negative Seebeck coefficient and conduct through the LUMO. These results support the initial predication that the transport mechanism of electrons is HOMO-dominated for OPE-1 and LUMO-dominated for other molecules. Secondly, the midgap mechanism points out that the position of Fermi energy is also a significant parameter because a small change in it could leads to different results for the thermopower.

The Seebeck coefficient was found to vary between 17.5 and −13 μV K^{-1} as shown in Table 3.5. Thermoelectric transport through OPE-backbone can be maintained despite the introduction of anchor points for side-group chemistry, and shows values in good consensus with the ones reported in literature for different anchoring groups, as well as The results obtained from detailed simulations based on density functional theory suggest that the sulfur atom of the anchoring groups coordinates to the electrode gold atoms in a very particular fashion.

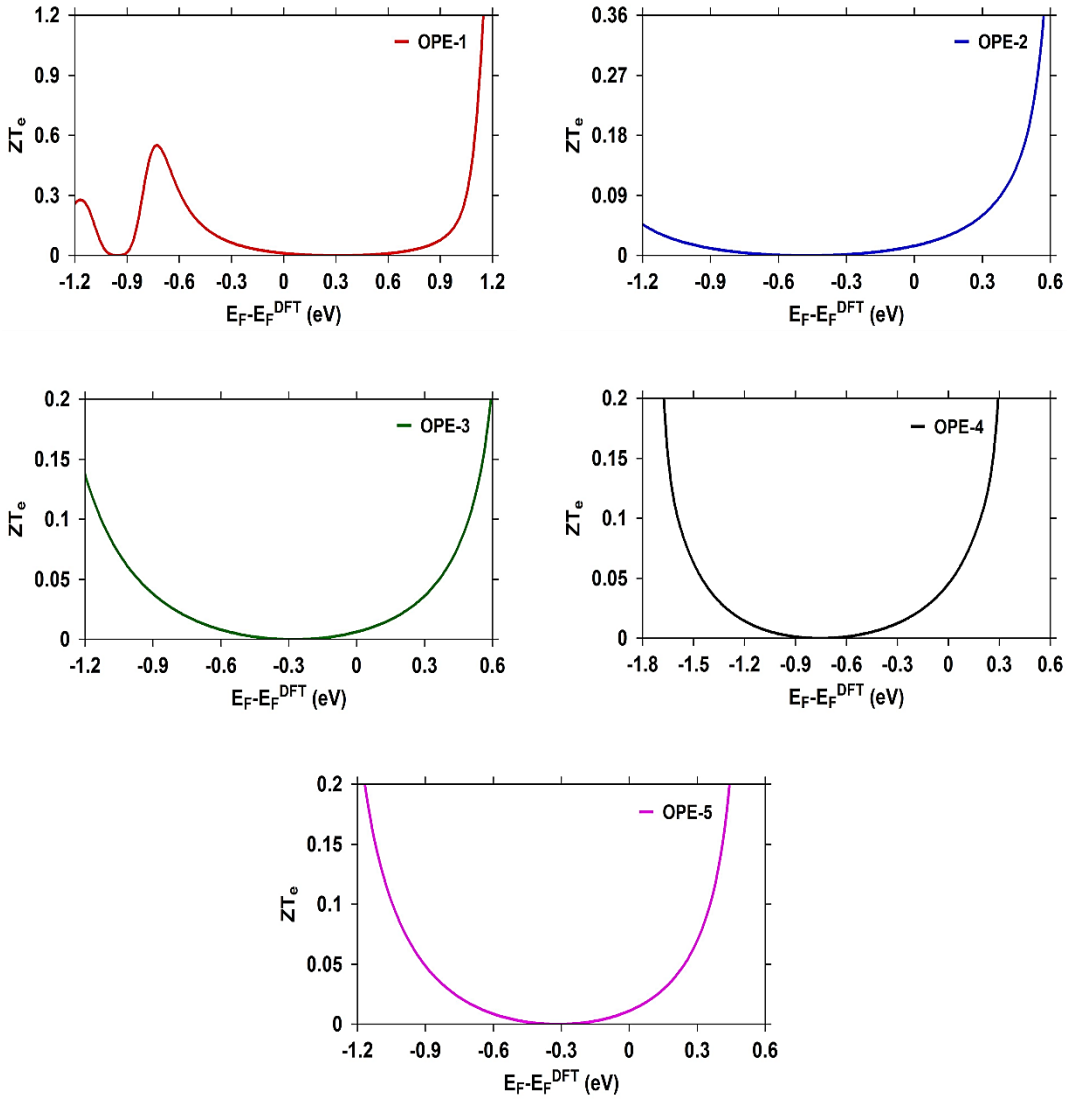

Figure 3.12. Represents the electronic figure of merit (ZT_e) as a function of Fermi energy for all molecules.

One of the most important parameters is the electronic figure of merit ZT_e. Therefore, I have calculated this parameter as shown in Figure 3.12. Thermoelectric materials convert thermal gradients and electric fields for power conversion and for refrigeration respectively.

With the increase in energy demand, thermoelectric applications are attracting a considerable interest. Unfortunately, thermoelectrics find currently only specialapplications due to their limited efficiency, which is

measured by a dimensionless parameter, the thermoelectric figure of merit: $ZT=S^2TG/k$, which includes the Seebeck coefficient (S), an average temperature T, the electrical conductance G, and the thermal conductance $k=k_{el}+k_{ph}$, the latter containing both electronic k_{el} and vibrational k_{ph} contributions. Maximizing ZT is challenging because optimizing one physical parameter often adversely affects another.

These results demonstrated again that the sign of Seebeck coefficient S for OPE-1 compounds is positive, while it is negative for other molecules. these results provided an excellent idea to design the molecular thermoelectric devices. Since, the molecule with SH anchor groups (OPE-1) gives the lowest ZT_e (0.01). While, the molecule with TMS anchor groups (OPE-4) produces the hieghest ZT_e (0.045), as shown in Table 3.5.

Table 3.5. The thermopower (S), and the electronic figure of merit (ZT_e).

Molecule	S (μVK^{-1})	ZT_e
OPE-1	17	0.012
OPE-2	-19	0.014
OPE-3	-13	0.006
OPE-4	-34	0.045
OPE-5	-17	0.011

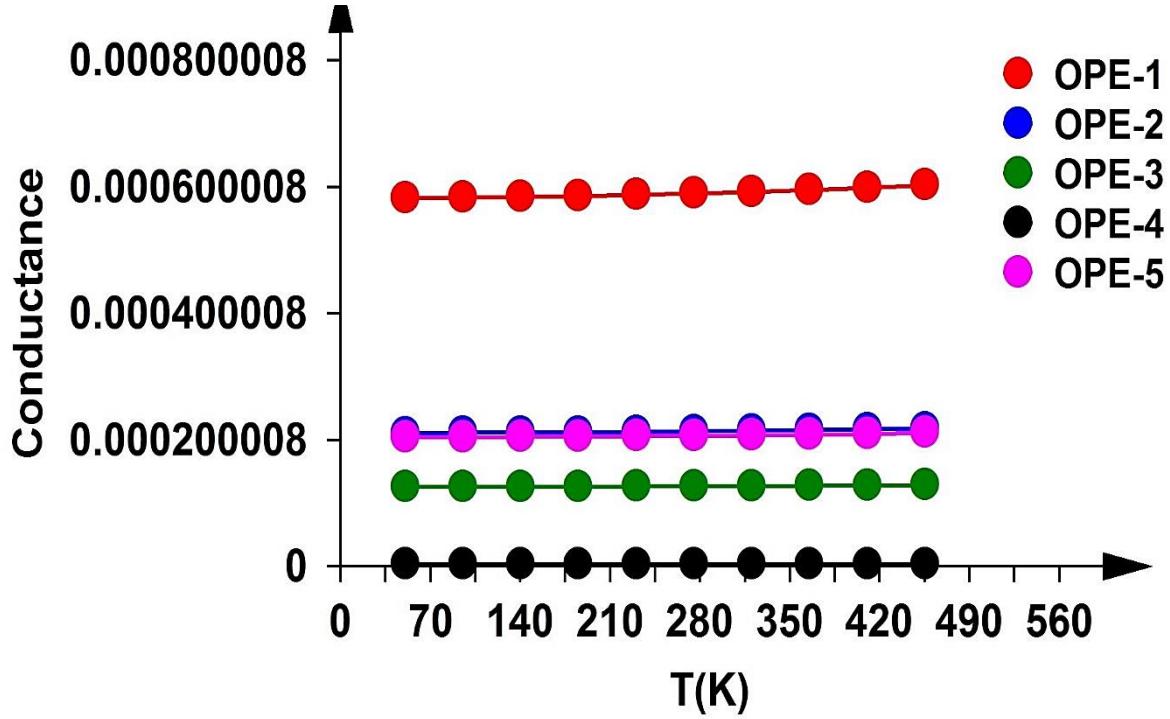

Figure 3.13. Represents the electrical conductance as a function of the temperature for all molecules.

These reults shown in Figure 3.13 have predicted that the tunneling conductance of single molecule junctions depends on temperature and can change slightly with changing the temperature from 50 K to 500 K. These calculations cannot be explained by changes in the Fermi distribution due to temperature smearing. However, it could be the structure of the metal-molecule interface changes with temperature slightly and propose that this factor can affect the tunneling transport through single molecule-metal junctions. At low temperatures, the electrodes remain highly corrugated and sharp, while at high temperatures the gold relaxes into a smoother geometry. This affects the alignment of the molecular orbitals relative to the metal Fermi level explaining the conductance shift with temperature observed here.

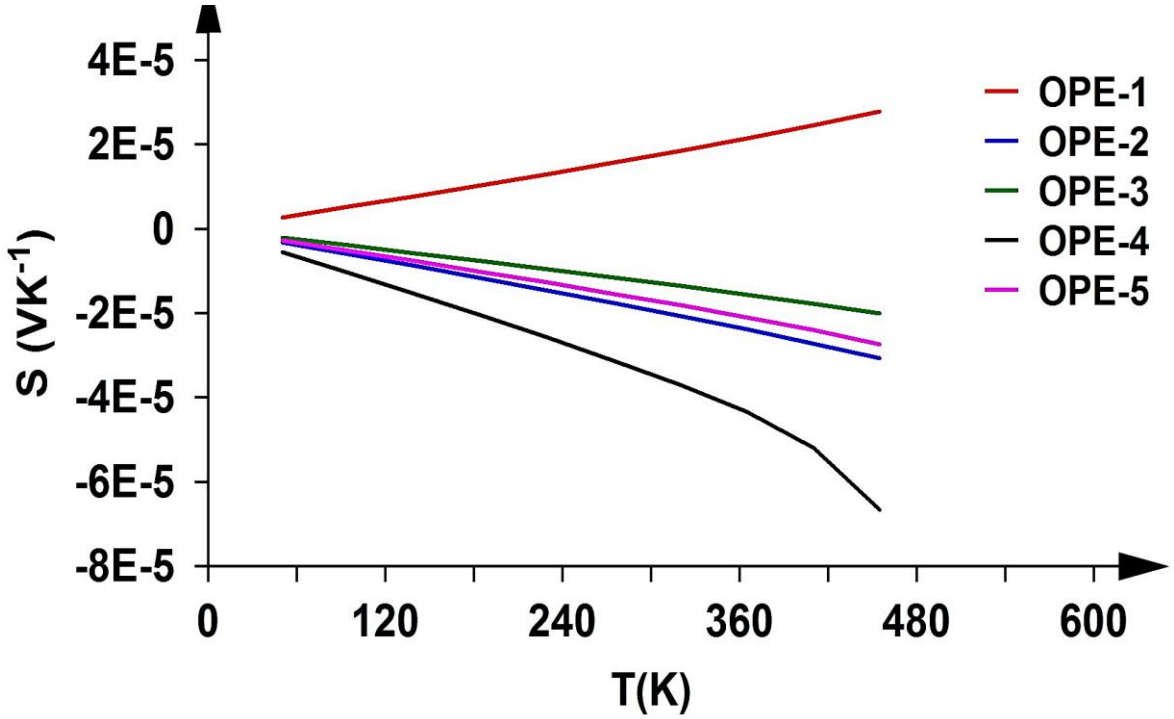

Figure 3.14. Represents the thermopower (S) as a function of the temperature for all molecules.

The calculations presented in Figure 3.14 show that the thermopower also slightly depends on the magnitude of the applied temperature, since the value of thermopower increased abit with increasing the temperature. Therefore, the main message here is that fluctuations, both thermal and from other sources (e.g., HOMO or LUMO position due to junction reconstruction), must be taken into account in calculations of thermopower and figure of merit of molecular junctions. On the other hand, there is no effect of the temperature on the sign of the thermopower. These results demonstrated that the structures of these molecules are robust and there is no sharp change in their electronic and thermoelectric properties under temperature fluctuations. Therefore, these molecules are best candiates for electronic applications.

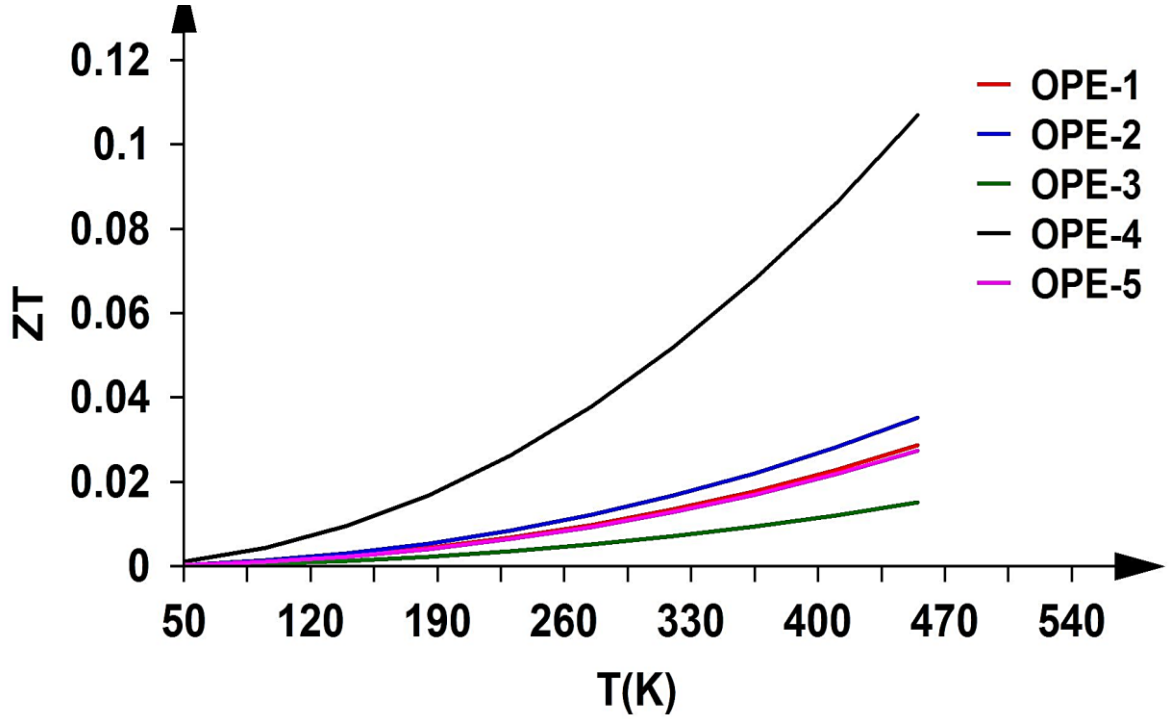

Figure 3.15. Represents the figure of merit (ZT) as a function of the temperature for all molecules.

Thermoelectric phenomena in unbiased metal-molecule junctions and other similar systems occur due to the difference in electrons distributions on the electrodes kept at different temperatures. The obtained results in Figure 3.15 shown that ZT reveals a strong dependence on the type of the anchor groups. Also, it may be affected by the fluctuations of the temperature which appear softly as an increasing in the value of the figure of merit.

Chapter Four

Conclusions and Future Works

4.1. Conclusions

In conclusion, this study using density functional theory methods have summarized systematic investigations on the effect of the anchoring group on electronic, spectral and thermoelectric properties of single-molecule junctions of several families of oligo(phenyleneethynylene) (OPE), with five different anchor groups (SH, PY, SMe, TMS and DBT).

The optimized molecular junction geometries conform well to a description of the SH, SMe and DBT contacted compounds forming an angle of 52º contact between anchor groups and the undercoordinated gold atoms of the gold electrodes. Also, it shows that PY and TMS contact groups create an angle of 160°, and produce an ideal junction formation probability.

The transmission coefficient value of all molecules is high. This can understand in terms of the quantum interference is a constructive interference and there is no a destructive interference signature. The order of the transmission is $T(E)_{OPE\text{-}1} > T(E)_{OPE\text{-}2} > T(E)_{OPE\text{-}5} > T(E)_{OPE\text{-}3} > T(E)_{OPE\text{-}4}$.

The molecule OPE-4 with TMS anchor gropus produces the highest f_{em} (2.4), while the molecule (OPE-2) with PY contact groups shows the lowest f_{em} (1.8). In addition, it could be observed that the maximum wavelength (λ_{max}) for all molecules lies in the UV region, and there is also a fluctuation from 349.7 nm for OPe-2 to 383.6 nm for OPE-5. Based on these results, we can

conclude that changing the anchor groups not only affects the transmission, but also the emission oscillator strength.

The thiol-terminated molecular junctions (OPE-1) have a positive Seebeck coefficient in agreement with transport and iso-surfaces calculations that show the HOMO is the molecular resonance that is closest to E_F. In contrast, SMe, DBT, PY and TMS-terminated molecular junctions have a negative Seebeck coefficient and conduct through the LUMO.

The molecule with SH anchor groups (OPE-1) gives the hieghest electronic properties and lowest thermoelectric properties. In contrast, the molecule with TMS anchor groups (OPE-4) produces the hieghest thermoelectric properties and the lowest electronic characteristics.

Based on the results that have been presented in this thesis, we can conclude that the strategy of changing the transport connecting groups from SH to PY or SMe or TMS or DBT not only affects the electronic and spectral aspects but also leads to a singnificant change in the thermoelectric properties of the single molecule junctions. Finally, this thesis introduces a successful and powerful strategy to develope the organic light-emitting diodes (OLEDs) in a single molecule technology, which can greatly simplify the display fabrication process and lead to new applications in electrically pumped organic lasers, and smart displays.

4.2. Future Works

Understanding transport characteristics of single metal−molecule−metal junctions is of fundamental importance to the development of functional nanoscale, organic-based devices. Therefore, I suggest some of ideas for the future work as follows:

1- Study the optical and spectral properties of several families of oligo(phenyleneethynylene) (OPE), with different side groups.
2- Investigation the electronic and thermoelectric properties of OPE molecules with different electrodes (carbon nanotubes and graphene).
3- Study the optoelectronics properties of OPE molecules with different anchor groups under magnetic field effects..

References

References

1. R. Martel, T. Schmidt, H. R. Shea, T. Hertel, and Ph. Avouris., Single- and Multiwall Carbon Nanotube Field-Effect Transistors. App. Phys. Lett., 1998. p. 2447–2449.

2. A. Kolmakov and M. Moskovits., Chemical Sensing and Catalysis by One-Dimensional Metal-Oxide Nanostructures. Annu. Rev. Mater. Res., 2004. p.151–180.

3. G. Raschke, S. Brogl, A. S. Susha, A. L. Rogach, T. A. Klar, J. Feldmann, B. Fieres, N. Petkov, T. Bein, A. Nichtl, and K. Kürzinger., Gold Nanoshells Improve Single Nanoparticle Molecular Sensors. Nano Lett., 2004. 4 (10) : p. 1853–1857.

4. M. C. Petty., Molecular Electronics: From Principles to Practice. John Wiley &Sons, Ltd., 2007.

5. J. R. Health and M. A. Ratner., Molecular electronics. Physics Today, 2003. P. 43–49.

6. D.Fichou, S. Delysse, and J.-M. Nunzi., First evidence of stimulated emission from a monolithic organic single crystal: α-Octithiophene. Adv. Mater. 1997.p. 1178–1181. 68

7. S. Chénais, and S. Forget., Recent advances in solid-state organic lasers. Polym. Int. 2012. p. 390–406.

8. M. A. Baldo, D. F. O'Brien, M. E. Thompson, and S. R. Forrest., Excitonic singlet-triplet ratio in a semiconducting organic thin film. Phys. Rev. 1999.p. 14422–14428.

9. C-S. Wang, A S. Batsanov, M. R. Bryce, S. Martin, R. J. Nichols, S. J. Higgins, V. M. García-Suárez and C. J. Lambert, Oligoyne Single Molecule Wires, Journal of the American Chemical Society 2009.

10. E. Leary, H. Höbenreich, S. J. Higgins, H. van Zalinge, W. Haiss, R.J. Nichols, C. Finch, I. Grace and C.J. Lambert, Single- molecule, solvation-shell sensing, Phys Rev. Lett. 2009.

11. GJ. Ashwell, B. Urasinska, C. Wang, MR. Bryce, I Grace, CJ. Lambert., Single-molecule electrical studies on a 7 nm long molecular wire‖ Chemical Communications, 2006, p. 4706-4708.

12. R. Huber, M. T. Gonzalez, S .Wu, M. Langer, S. Grunder, V. Horhoiu, M. Mayor, M. R. Bryce, C. S. Wang, R. Jitchati, C. Schonenberger, M. Calame, J. Am. Chem., Soc. 2008, p. 130, 1080-1084.

13. W. Hong, D. Z. Manrique, P. Moreno-Garca, M. Gulcur, A. Mishchenko, C. J. Lambert, M. R. Bryce, T. J. Wandlowski, Am. Chem. Soc. 2011, 134, p.2292-2304.

14. H. Sadeghi, S. Bailey, CJ. Lambert., Silicene-based DNA nucleobase sensing, Applied Physics Letters 2014, 104 (10), p.103-104 .

15. R. Martel, et al., Single- and multi-wall carbon nanotube field-effect transistors. Applied Physics Letters, 1998. 73 (17): p. 2447-2449.

16. A. DeHon, Array-based architecture for FET-based, nanoscale electronics. IEEE Transactions on Nanotechnology, 2003. 2 (1): p. 23-32.

17. Z.J Donhauser, et al., Conductance Switching in Single Molecules Through Conformational Changes. Science, 2001. 292 5525: p. 2303.

18. C. Wang, et al., Ultrathin Au nanowires and their transport properties. J Am Chem Soc, 2008. 130(28): p. 8902-3.

19. M. Tsutsui, and M. Taniguchi, Single Molecule Electronics and Devices. Sensors Basel, Switzerland, 2012. 12(6): p. 7259-7298.

20. R. Waser, and M. Aono., Nanoionics-based resistive switching memories. Nature Materials, 2007. 6: p. 833.

21. P. Franzon, et al., Molecular Electronics – Devices and Circuits Technology, in Vlsi-Soc: From Systems To Silicon: Proceedings of IFIP TC 10, WG 10.5, Thirteenth International Conference on Very Large Scale Integration of System on Chip (VLSI-SoC 2005), October 17-19, 2005, Perth, Australia, R. Reis, A. Osseiran, and H.-J. Pfleiderer, Editors. 2007, Springer US: Boston, MA. p. 1-10.

22. M.C. Petty, et al., Molecular Electronics, in Springer Handbook of Electronic and Photonic Materials, S. Kasap and P. Capper, Editors. Springer International Publishing: Cham. 2017. p. 1-1.

23. J. Gierschner, S. Varghese, and S. Y. Park, Organic single crystal lasers.: a materials view. Adv. Opt. Mater. 2016. 4, p. 348–364.

24. C. Robert, Jr. Neuman, Organic Molecules and Chemical Bonding. G. Somasundaram and A. Ramalingam, Chem. Phys. Lett.,2000, 324, p. 25–30.

25.Changsheng Wang, Andrei S. Batsanov and Martin R. Bryce. ,Oligoyne Single Molecule Wires. . J.of the American Chemical Society. 2009, 131,p. 15647–15654.

26. Pavel M. García, Murat G.and David Z. Manrique. Single-Molecule Conductance of Functionalized Oligoynes: Length Dependence and Junction Evolution. J.of the American Chemical Society. July 22, 2013.

27. Oday A. Al-Owaedi, David C. Milan, Marie-Christine Oerthel, Sören Bock, Dmitry S. Yufit, Judith A. K. Howard, Simon J. Higgins, Richard J. Nichols, Colin J. Lambert, Martin R. Bryce, Paul J. Low." Experimental and Computational Studies of the Single-Molecule Conductance of Ru(II) and Pt(II) trans-Bis(acetylide) Complexes. Organometallics," 2016, 35, p. 2944−2954.

28. Oday A. Al-Owaedi, Sören Bock, David C. Milan, Marie-Christine Oerthel, Michael S. Inkpen, Dmitry S. Yufit, Alexandre N. Sobolev, Nicholas J. Long, Tim Albrecht, Simon J. Higgins, Martin R. Bryce, Richard J. Nichols, Colin J. Lambert, Paul J. Low., Insulated molecular wires: inhibiting orthogonal contacts in metal complex based molecular junctions. Nanoscale,. 2017, 9, p. 9902–9912.

29. Mohsin Kadhim Abed Al-Khaykanee., Quantum Theory of Electronic and Thermal Transport through Nano-scale and Single-Molecule Devices. Department of Physics, Lancaster University, UK Ph.D. Thesis 2018.

30. P. Guang- Zhanga, Yan-Qi Mua, Jin-M. Zhaoa and Hui Huang., Optimizing the conductance switching performance in photo switchable dimethyldihydropyrene/cyclophanediene single-molecule junctions. Physica E: Low-dimensional Systems and Nanostructures. 2019.

31.Masoud Baghernejad, Yang Yang and Oday A. Al-Owaedi. ,Constructive Quantum Interference in Single-Molecule Benzodichalcogenophene Junctions. Chemistry - A European Journal • February 2020.

32.Yi Jiang, Yuan-Y. Liu, Xu Liu, He Lin and Kun Gao., Organic solid-state lasers: a materials view and future development. Chem Soc RevDOI: 2020.10.1039/d0cs00037j.

33. Baraa A. Al-Mammory, Oday A. Al-Owaedi, Enas M. Al-Robayi. ,Thermoelectric Properties of Oligoyne-Molecular Wires. J. of Phys. Conference Series. 2021.p. 1818. 012095

34. Rasool M. Al-Utayjawee, Oday A. Al-Owaedi., Enhancement of Thermoelectric Properties of Porphyrinbased Molecular Junctions by Fano Resonances. J. of Phys. Conference Series .2021. p.1818,. 012208.

35. M. Naher et al., Molecular Structure–Thermo electric Property Relationships in Single-Molecule Junctions and Comparisons with Single-and Multiple-Parameter Models,.J. Am. Chem. Soc., , 2021. 143(10), p. 3817–3829.

36. Bensalem Salaheddine, .Contribution to the study of physical properties of CZTX (X=S, Se) solar materials. Ph.D Thesis, Department of Physics, Faculty of Sciences. University Ferhat Abbas, Algeria, (2015).

37. P. Hohenberg and W. Kohn, .Inhomogeneous Electron Gas., Phys. Rev.B 1964 136, p. 864-871 .

38. W. Kohn and L. J. Sham, .Self-Consistent Equations Including Exchange and Correlation Effects. Phys. Rev. A 140, 1965 p. 1133-1138.

39. N. Argaman and G. Makov., Density Functional Theory – an introduction., American Journal of Physics, arXiv.org:physics/9806013 1999.

40. M. Born, and R. Oppenheimer, On the quantum theory of molecules. Annalen der Physik, 1927. 84(20): p. 1–32.

41. Mel Levy. Universal variational functionals of electron densities, first order density matrices, and natural spin-orbitals and solution of the v-representability problem. Proc. Natl. Acad. Sci. USA. 1979. 76(12): p. 6062–6065.

42. M. R. Dreizler, and J. Providencia., Density functional methods in physics. NATO ASI series. Series B, Physics, 1985.

43. R.G. Parr, and Y. Weitao, Density-functional theory of atoms and molecules. Oxford University Press, USA. 1994. 16.

44. E. K. Gross, and R. M. Dreizler, Density functional theory. Springer, 1995.

45. Levy, M. Electron densities in search of Hamiltonians. Physical Review A, 1982. 26(3): p. 1200–1208.

46. E. H. Lieb., Thomas-Fermi and related theories of atoms and molecules. Reviews of Modern Physics, 1981. 53(4): p. 603–641.

47. Hartree, D. R. Proc. Cam. Phil. Soc. 1928. 24. p. 89–110.

48. Hartree, D. R. Proc. Cam. Phil. Soc. 1928. 24. p.111–132.

49. Hartree, D. R. Proc. Cam. Phil. Soc. 1928. 24. p.426–437.

50. Fock, V. Z. Physik., 1930. 61. p. 126–148.

51. D. R. Hartree., the Calculation of Atomic Structures; Structure of Matter Series; John Wiley & Sons Ltd. London, 1957.

52. D. Axel, Becke., Density-functional exchange-energy approximation with correct asymptotic behavior. Physical Review A, 1988. 38(6): p. 3098–3100.

53. C. L. David, and J. P. Perdew., The exchange-correlation energy of a metallic surface. Solid State Communications, 1975. 17(11): p. 1425–1429.

54. B. Hammer, L. B. Hansen, J. K. Nørskov., Improved dsorption energetics within density-functional theory using revised perdew-burke-ernzerhof functionals. Physical Review B, 1999. 59(11): p. 7413–7421.

55. Richard M. Martin. Electronic structure: basic theory and practical methods. Cambridge university press, 2004.

56. D. M. Ceperley, and B. Alder., Ground state of the electron gas by a stochastic method. Physical Review Letters, 1980. 45(7): p. 566–569.

57. J. P. Perdew, and A. Zunger., Self-interaction correction to density-functional approximations for many-electron systems. Physical Review B, 1981. 23(10): p. 5048–5079.

58. R. Q. Hood, M. Y. Chou, A. J. Williamson, G. Rajagopal and R. J. Needs. Quantum Monte Carlo investigation of exchange and correlation in silicon. Phys. Rev. Lett. 1997. 78(17): p. 3350–3353.

59. R. Q. Hood, M. Y. Chou, A. J. Williamson, G. Rajagopal and R. J. Needs. Exchange and correlation in silicon. Physical Review B, 1998. 57(15): p. 8972–8982.

60. R. Car., Quantitative Structure-Activity Relationships. 2002. 21(2): p. 97–104.

61. P. Fulde., Electron Correlations in Molecules and Solids. 1995. Springer.

62. L. Hedin, and S. Lundqvist., Effects of electron-electron and electron-phonon interactions on the one-electron states of solids. Solid State Physics, 1970. 23: p. 1–181.

63. S. H. Vosko, L. Wilk, and M. Nusair., Accurate spin-dependent electron liquid correlation energies for local spin density calculations: a critical analysis. Canadian Journal of Physics, 1980. 58(8): p. 1200–1211.

64. J. P. Perdew, K. Burke, and M. Ernzerhof., Generalized gradient approximation made simple. Physical Review Letters, 1996. 77(18): p. 3865–3868.

65. J. P. Perdew, A. Ruzsinszky, J.Tao, V. N. Staroverov, G. E. Scuseria, G. I. Csonka., Prescription for the design and selection of density functional approximations: More constraint satisfaction with fewer fits. The Journal of Chemical Physics, 2005. 123(6): p. 062201–062209.

66. D. Z. Manrique, C. Huang, M. Baghernejad, X. Zhao, Al-Owaedi, O. A.; H. Sadeghi, V. Kaliginedi, W. Hong, M. Gulcur, T. Wandlowski, M. Bryce, R. and Lambert, C. J. A Quantum Circuit Rule for Interference Effects in Single-Molecule Electrical Junctions. Nat. Commun. 2015. 6(6389): p. 1–8.

67. Ross, Davidson; Oday, A. Al-Owaedi; David, C. Milan; Qiang, Zeng; Joanne, Tory; František, Hartl; Simon, J. Higgins; Richard, J. Nichols; Colin, J. Lambert and Paul, J. Low. Effects of Electrode−Molecule Binding and Junction Geometry on the Single-Molecule Conductance of bis-2,2′:6′,2″-Terpyridine-based Complexes. Inorg. Chem. 2016. 55(6): p. 2691–2700.

68. David, C., Milan; Oday, A., Al-Owaedi; Marie-Christine, Oerthe; Santiago, Marqués-González; Richard, J., Brooke; Martin, R., Bryce; Pilar, Cea; Jaime, Ferrer; Simon, J., Higgins; Colin, J., Lambert; Paul, J., Low; David, Zsolt, Manrique; Santiago, Martin; Richard, J., Nichols; Walther,

Schwarzacher and Víctor, M. García-Suárez. J. Phys. Chem. C, 2016. 120(29): p. 15666–15674.

69. O. F. Sankey, and D. J. Niklewski., Ab initio multicenter tight-binding model for molecular-dynamics simulations and other applications in covalent systems. Physical Review B, 1989. 40(6): p. 3979–3995.

70. S. Botti., Applications of Time-Dependent Density Functional Theory. IOP Science, Physica Scripta, 2004 (109), p. 54-60.

71. M. Petersilka, U. J. Gossmann and E. K. U. Gross, .Excitation Energies from Time-Dependent Density-Functional Theory. Physical Review Letters, 1996. 76(8), p. 1212-1215.

72. A. Szabo and N. S. Ostlund, .Modem quantum chemistry: Introduction to advanced electronic structure theory. Dover Publication, Inc. Mineola, New York, 2012. p. 484.

73. R. Chandiramouli., Structural and electronic properties of germanane nano-sheet upon molecular adsorption of alcohol and aldehyde molecules: DFT comparative analysis. Elsevier, Journal of Molecular Liquids, 2017. 242, p. 571-579.

74. W. J. Hehre, .A Guide to Molecular Mechanics and Quantum Chemical Calculations. Wave function, Inc., Printed in the USA, 2013.p. 796.

75. C. A. Tsipis., DFT flavor of coordination chemistry", Elsevier, Coordination Chemistry Reviews, 2014. 272, p. 1-29.

76. N. E. Economou,. Green's functions in quantum physics. Book, 3rd Edition, Springer Series in Solid-State, 2006. p. 474.

77. M. Büttiker, Y. Imry, R. Landauer, S. Pinhas., Generalized many-channel conductance formula with application to small rings. Physical Review b 1985. 31 6207.

78. S. Datta., Electronic transport in mesoscopic systems. (Cambridge university press, 1995.

79. Negele J W and Orland H Quantum Many-Particle Systems (New York Perseus Book Group) 1998.

80. S. Datta., Electronic transport in mesoscopic systems :Cambridge university press, 1997.

81. N. R. Claughton, M. Leadbeater, and C. J. Lambert, Theory of Andreev Resonances in Quantum Dots, Journal of Physics-Condensed Matter, 1995. 7(46), p. 8757– 8784.

82. Sankey, F. Otto and J. David Niklewski,. Ab initio multicenter tight-binding model for molecular-dynamics simulations and other applications in covalent systems. Physical Review B 40, no. 6 .1989 : 3979.

83. L. A. Algharagholy, Q. Al-Galiby, H. A. Marhoon, H. Sadeghi, H. M.

Abduljalil, and C. J. Lambert, .Tuning thermoelectric properties of graphene/boron nitride heterostructures. Nanotechnology, 2015. 26(47) p. 475401.

84. C.-X. Liu, X.-L. Qi, H. Zhang, X. Dai, Z. Fang, and S.-C. Zhang., Model Hamiltonian for topological insulators. Phys. Rev. B, 2010. 82 (4), p. 45122.

85. S. Mao, A. Yamakage, and Y. Kuramoto., Tight-binding model for topological insulators: Analysis of helical surface modes over the whole Brillouin zone. Phys. Rev. B, 2011. 84(11), p. 115413.

86. S. Barraza-Lopez and T. P. Kaloni., Water splits to degrade twodimensional group-IV monochalcogenides in nanoseconds. ACS Cent. Sci., 2018. 4(10) p. 1436–1446.

الخلاصة

إن لفهم نقل الشحنة للجزيئات المفردة المحصورة بين الأقطاب الكهربائية له أهمية أساسية للإلكترونيات الجزيئية. الخصائص التركيبية للأوليغو (فينيلين إيثيلين)(OPE) مع خمس مجموعات ربط مختلفة (SH, PY, SMe, TMS and DBT). تتوافق هندسة الوصلات الجزيئية المحسّنة جيدًا مع وصف المركبات الملامسة لـ SH و SMe و DBT التي تشكل زاوية تلامس 52 درجة بين مجموعات الربط وذرات الذهب المنسقة. أيضًا، يُظهر أن مجموعات جهات الاتصال PY و TMS تنشئ زاوية 160 درجة. مما لا شك فيه أن هذه الجوانب الهيكلية ستؤثر على احتمالية تكوين الوصلة وجميع الخصائص الأخرى (الإلكترونية والكهربائية والحرارية والطيفية) لهذه الجزيئات. من ناحية أخرى ،فأن قيمة معامل النقل لجميع الجزيئات عالية. ومن هذا يمكن أن نفهم أن التداخل الكمي هو تداخل بناء ولا يوجد أي حدوث للتداخل الهدام، وأن (OPE-1) يعطي قيمة عالية لمعامل الانتقال (5.8×10^{-4}) ، بينما يعطي أقل قيمة لمعامل الإنتقال (3.12×10^{-6}) بواسطة الجزيء (OPE-4). ينتج الجزيء OPE-4 مع مجموعة الربط TMS أعلى f_{em} (2.4)، بينما يُظهر الجزيء (OPE-2) مع مجموعات التلامس PY أقل مستوى f_{em} (1.8).

بالإضافة إلى ذلك ، يمكن ملاحظة أن أقصى طول موجي (λmax) لجميع الجزيئات يكمن في المنطقة المرئية ، وهناك أيضًا تذبذب من 349.7 نانومتر لـ OPE-2 إلى 383.6 نانومتر لـ OPE-5. من ناحية أخرى، فإن الوصلات الجزيئية المنتهية بالثيول (OPE-1)لها معامل سيبيك موجب الذي يُوضح HOMO. في المقابل ، فإن الوصلات الجزيئية المنتهية بـ SMe و DBT و PY و TMS لها معامل سيبيك سالب موضح من خلال لـ LUMO .يعطي الجزيء الذي يحتوي على مجموعات ربط SH (OPE-1) أعلى خصائص إلكترونية وأقل خصائص كهروحرارية. في المقابل، ينتج الجزيء

الذي يحتوي على مجموعات ربط TMS (OPE-4) أعلى خصائص كهروحرارية وأقل خصائص إلكترونية.

جمهورية العراق
وزارة التعليم العـالي والبحث العلـمي
جامـــعة بـــابـــل
كليـــة العلـوم للبنات
قســـم فيزيـــاء الليزر

الدراسة النظري لخصائص الإلكترونيات الضوئية لجزيئات أليغو (فينيلين إيثينلين) لصبغ الليزر العضوي

أطروحة مقدمة

الى مجلس كلية العلوم للبنات في جامعة بابل

وهي جزء من متطلبات نيل درجة الماجستير في علوم فيزياء الليزر وتطبيقاته

من قبل الطالبة
نور مدين عظيم
بأشراف

أ.م.د عدي اركان عباس الجبوري

٢٠٢٢م **١٤٤٣ هـ**